Published OnlineFirst February 24, 2011; DOI:10.1158/0008-5472.CAN-10-3524

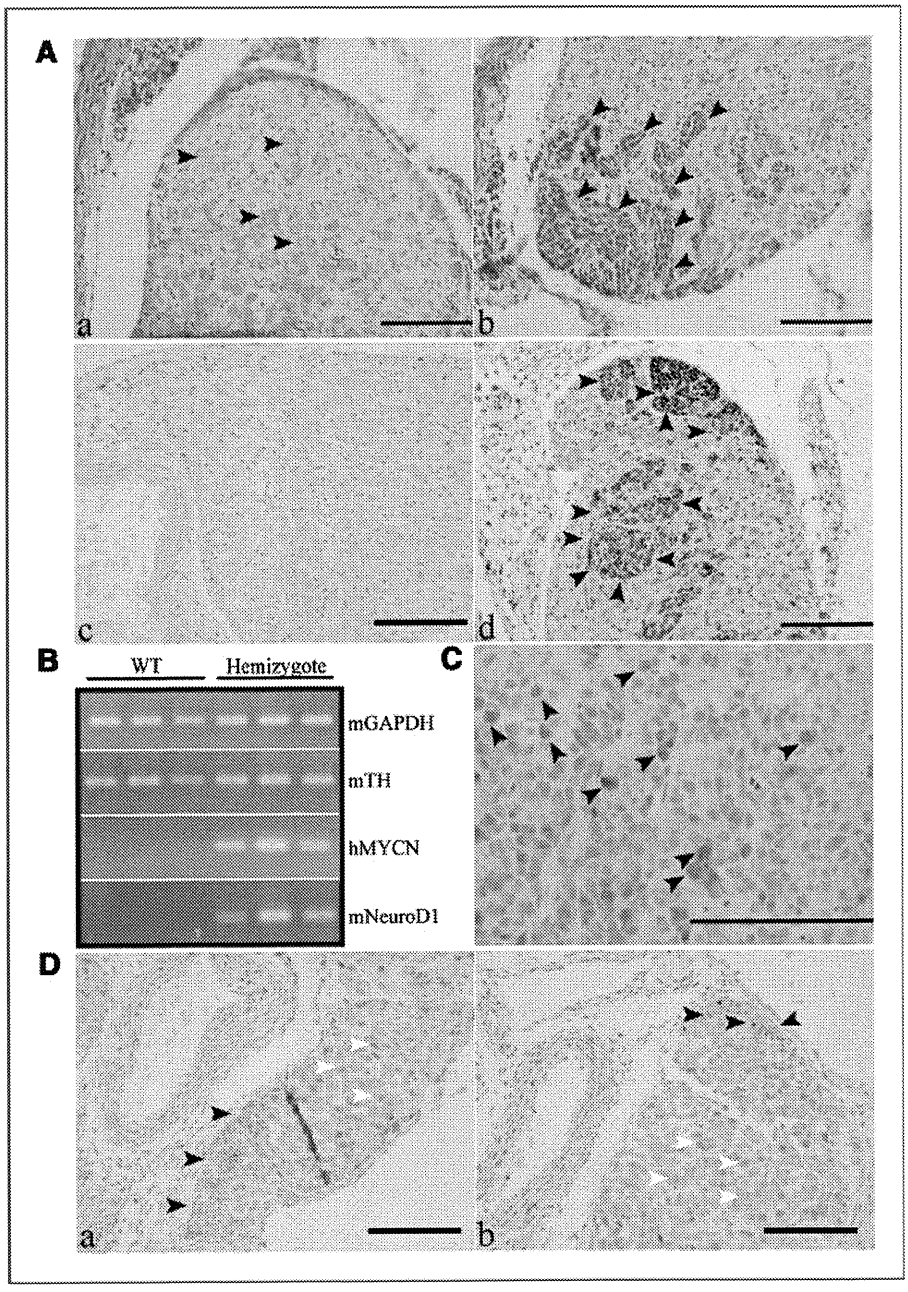

Figure 1. Expression of NeuroD1 in the mouse hyperplastic ganglion and tumor. A, the celiac sympathetic ganglions from 2-week-old WT (a) and *MYCN* hemizygote (b) mice. Normal ganglion cells show large nuclei (arrowheads in a). Neuroblast hyperplasia appears as clusters of basophilic, small round neuroblasts (arrowheads in b). c and d, immunochemical staining of NeuroD1 in 2-week-old WT (c) and *MYCN* hemizygote mice (d). Arrowheads in d indicate hyperplastic regions. B, RT-PCR for NeuroD1 expression in ganglions. C, immunochemical staining of NeuroD1 in tumor. Cells strongly expressing NeuroD1 are indicated by arrowheads. D, immunochemical staining for NeuroD1 at day 0 in WT (a) and *MYCN* hemizygote (b) mice. Black arrowheads indicate hyperplastic regions, and white ones indicate immature ganglion cells. Scale bar, 100 μm. GAPDH, glyceraldehyde 3-phosphate dehydrogenase.

[Fig. 1D (a and b), black arrowheads]. These results indicate that the hyperplasia at 2 weeks in *MYCN* Tg mice is different from that at day 0 in both WT and *MYCN* Tg mice. Thus, NeuroD1 expression is switched on in hyperplastic regions in *MYCN* Tg mice during the first 2 weeks after birth.

NeuroD1 is involved in cell motility

The *in vivo* expression profile suggests a possible involvement of NeuroD1 in NB tumorigenesis or development. To examine this hypothesis, we investigated the role of NeuroD1 in NB cells. In the *MYCN* amplified cell line IMR32, NeuroD1 expression was significantly suppressed by 2 shRNAs acting against human NeuroD1 that were transiently expressed via a lentivirus expression system (Fig. 2A). Although there was no difference in cell growth between the control shRNA and NeuroD1 shRNA-treated cells, we found that NeuroD1 shRNAs inhibited cell motility in a scratch assay (Fig. 2A). Furthermore, we found that SH-SY5Y cells, a human NB cell line without *MYCN* amplification, showed a high level of NeuroD1 expression (Fig. 2B; Supplementary Fig. S1). In addition, NeuroD1 shRNA

Published OnlineFirst February 24, 2011; DOI:10.1158/0008-5472.CAN-10-3524

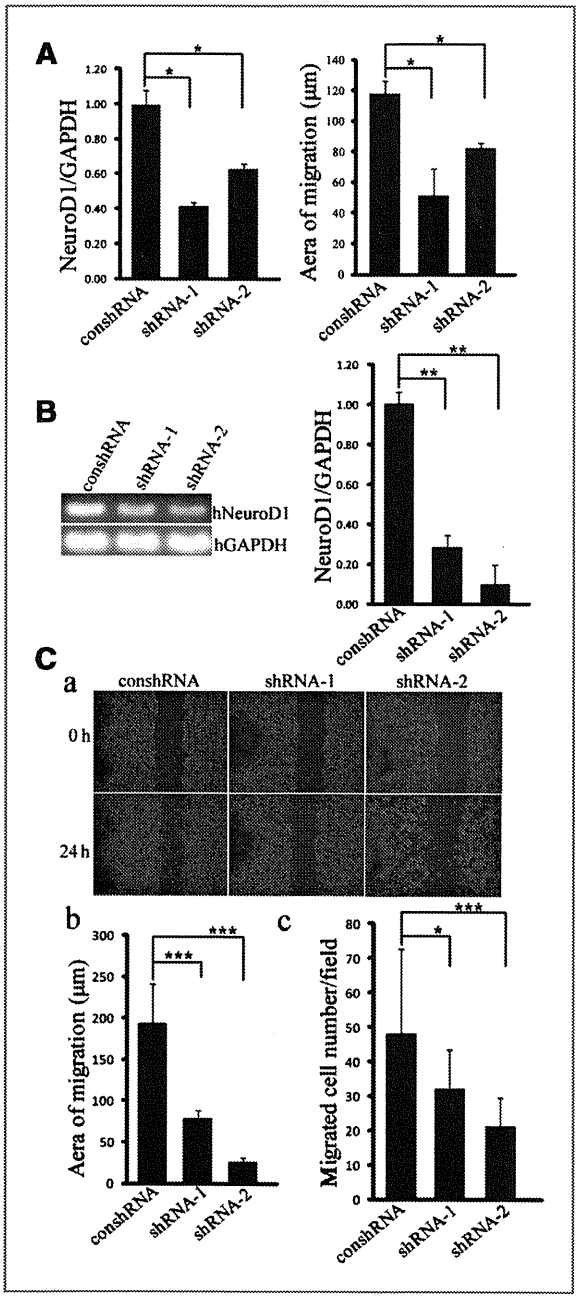

Figure 2. Transient knockdown of NeuroD1 leads to motility inhibition of IMR32 cells and SH-SY5Y cells. A, a quantitative RT-PCR showed significant decrease in NeuroD1 expression by 2 lentivirus-based shRNAs against NeuroD1 in IMR32 cells (left). Directional cell migration of IMR32 cells was evaluated by wound-healing assay (right). B, RT-PCR and quantitative PCR results showing efficient knockdown of NeuroD1 by the 2 shRNAs in SH-SY5Y cells. C, a and b, directional cell migration of SH-SY5Y cells was evaluated by wound-healing assay. c, migration of SH-SY5Y cells was evaluated by the Boyden chamber assay. *, $P < 0.05$; **, $P < 0.01$; ***, $P < 0.001$ (Student's *t* test). GAPDH, glyceraldehyde 3-phosphate dehydrogenase.

effectively suppressed NeuroD1 expression (Fig. 2B) and inhibited cell motility in a scratch assay [Fig. 2C (a and b)]. In support of these data, we report that a Boyden chamber cell migration assay showed NeuroD1 shRNA-mediated inhibition [Fig. 2C (c)].

Next, we established cells in which NeuroD1 shRNA or control shRNA was stably expressed, such that we could perform rescue experiments and analyze the underlying molecular mechanism. The established NeuroD1-knockdown cells showed a significantly suppressed expression of NeuroD1 (Fig. 3A). The NeuroD1 shRNA-treated cells became round, which was strikingly different from that of the shape of parent cells (Fig. 3B). However, data obtained with regard to cell growth and cell-cycle analyses showed that cell growth was comparable between the control shRNA cells and NeuroD1 shRNA-treated cells (Supplementary Fig. S2). As expected, a scratch assay revealed that NeuroD1 shRNA-treated cells showed less motility (Fig. 3C). This inhibition was observed up to 72 hours after scratch (Supplementary Fig. S3). This phenomenon was attributed to the knockdown of NeuroD1 expression, because the shRNA-resistant NeuroD1 expression reversed the NeuroD1 shRNA-induced suppression of cell motility (Fig. 3D).

NeuroD1 downregulates Slit2 expression

What is the underlying mechanism? Coincidentally, we found that Slit2 mRNA expression was induced by knockdown of NeuroD1 expression in both IMR32 cells and SH-SY5Y cells (Fig. 4A). Consistent with this finding, SH-SY5Y cells stably expressing NeuroD1 shRNA were found to express the Slit2 protein at a much higher level than cells expressing the control shRNA (Fig. 4B). It is of importance that shRNA-resistant NeuroD1 expression in the NeuroD1 shRNA-treated cells significantly suppressed Slit2 protein expression (Fig. 4B).

It is known that NeuroD1 is a transcription factor that binds to the E-box in the regulatory region of target genes (22). Therefore, in the next step, we explored whether NeuroD1 was recruited to the regulatory region of the human *Slit2* gene. There are 6 E-box stretches surrounding the *Slit2* gene (Fig. 4C). A ChIP assay revealed that NeuroD1 directly bound to the first and second E-box but not to the other E-boxes (Fig. 4D).

NeuroD1 knockdown led to the inhibition of cell motility and an increase in Slit2 expression and therefore Slit2 might possibly be involved in cell motility. To test this hypothesis, we knocked down Slit2 expression in the cells expressing NeuroD1 shRNA. shRNAs functioning against human Slit2 efficiently suppressed Slit2 expression in NeuroD1 shRNA-treated cells (Fig. 5A). These double-knockdown cells restored cell motility (Fig. 5B and C), and this supports the hypothesis that NeuroD1 promotes cell motility by suppressing Slit2 expression. When we knocked down only Slit2 expression in SH-SY5Y cells, cell motility was enhanced (Supplementary Fig. S4).

NeruoD1 knockdown suppresses tumor sphere growth and tumor growth

To further examine the functional relevance of NeuroD1 to tumorigenesis, we knocked down NeuroD1 expression in tumor spheres established from NB tumor tissue derived from *MYCN* Tg mice. We examined 2 shRNAs against mouse

Published OnlineFirst February 24, 2011; DOI:10.1158/0008-5472.CAN-10-3524

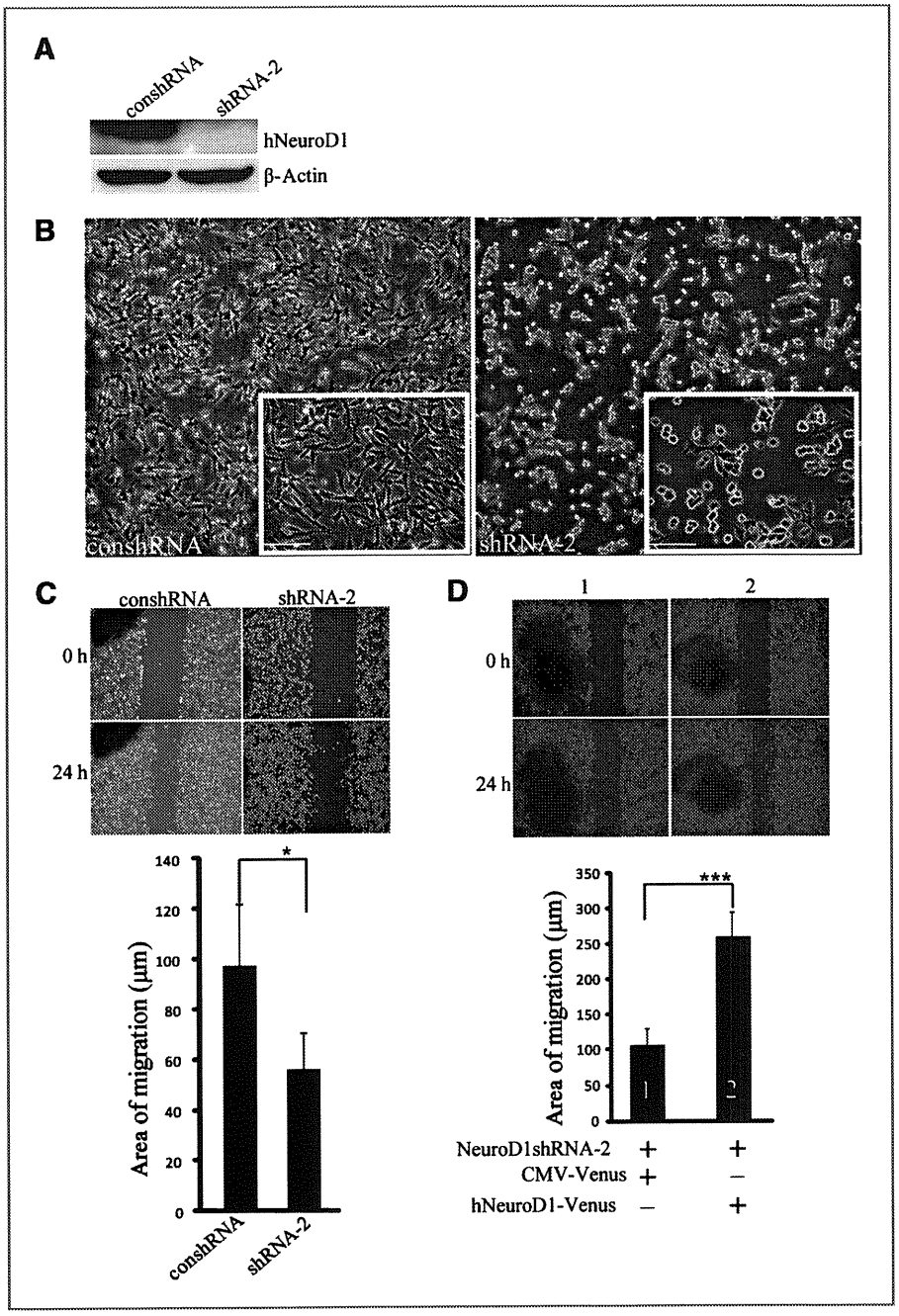

Figure 3. Stable knockdown of NeuroD1 leads to motility inhibition. A, the whole-cell extract of SH-SY5Y stably expressing control shRNA (conshRNA) or NeuroD1 shRNA-2 was subjected to Western blot analysis. B, phase-contrast photographs showing the shape change induced by NeuroD1 knockdown. Insets show higher magnification. C, wound-healing assay of SH-SY5Y cells stably expressing conshRNA or NeuroD1 shRNA-2. D, shRNA-resistant human NeuroD1 restores the motility of NeuroD1 shRNA SH-SY5Y cells. Cells indicated as 1 and 2 in D were treated as follows: 1, NeuroD1 shRNA-2 and CMV-Venus plasmid; 2, NeuroD1 shRNA-2 and hNeuroD1-Venus plasmid. Scale bar, 50 μm. * $P < 0.05$, *** $P < 0.001$ (Student's t-test).

NeuroD1. They efficiently suppressed NeuroD1 expression in tumor spheres after infection via a lentiviral system (Fig. 6A). Control shRNA-expressing tumor spheres showed a tightly packed shape and thus the interface between cells was nearly invisible (Fig. 6A). In contrast, cell–cell contact in the NeuroD1-knockdown tumor spheres appeared loose (Fig. 6A). Furthermore, NeuroD1 shRNAs strongly suppressed the growth of tumor spheres (Fig. 6B). Effects of NeuroD1 on sphere self-renewal ability are shown in Figure 6C. Primary and secondary sphere-formation ability was impaired after NeuroD1 knockdown when evaluated by sphere number (Fig. 6C). In addition, NeuroD1 knockdown spheres were smaller (Fig. 6C).

The NeuroD1 functions, that is, cell motility and tumor sphere growth, revealed during this study further support the idea that NeuroD1 might be involved in NB tumor development. To examine this idea, we injected 1×10^4 cells from tumor spheres, which had been infected with lentivirus

Published OnlineFirst February 24, 2011; DOI:10.1158/0008-5472.CAN-10-3524

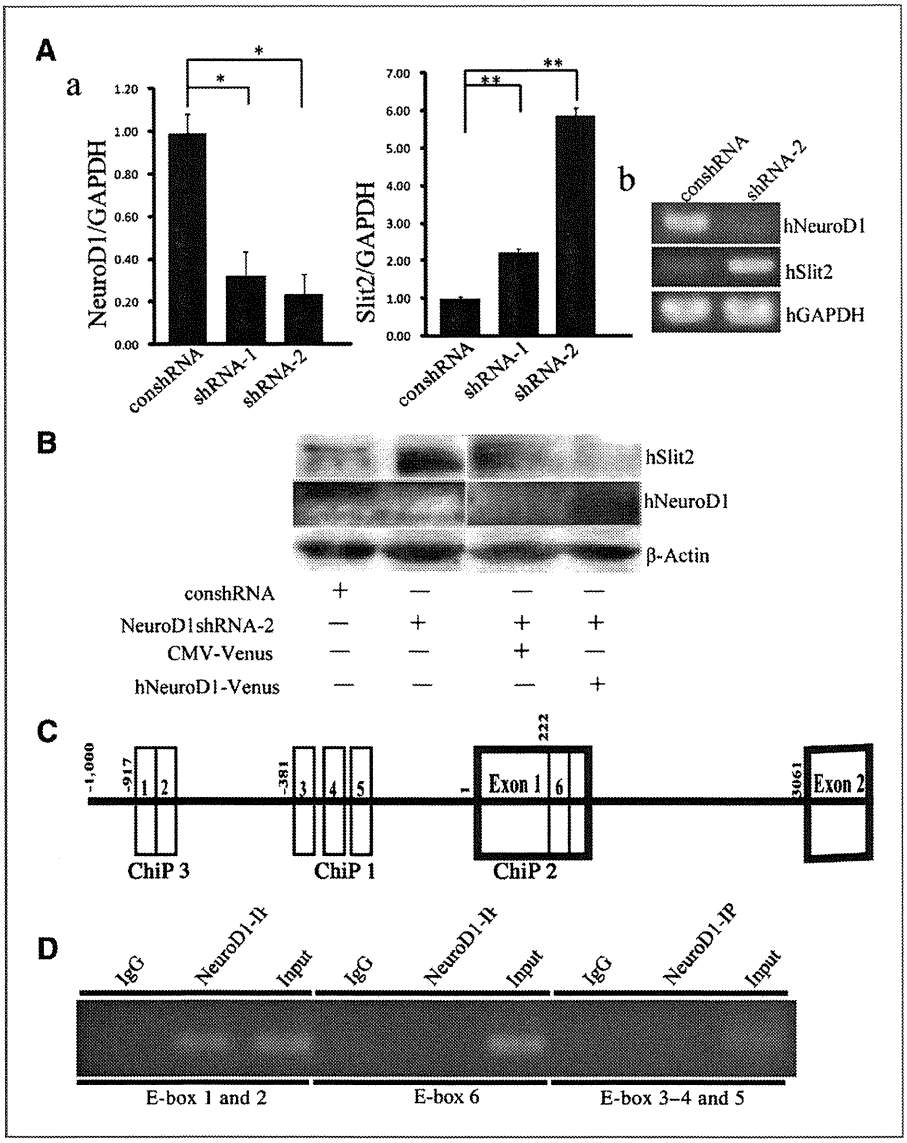

Figure 4. Reverse expression of NeuroD1 and Slit2. A, the RT-PCR results indicate the inverse relationship between NeuroD1 and Slit2 expression. a, IMR32 cells; b, SH-SY5Y cells. B, Western blot analysis for Slit2 and NeuroD1 expression in NeuroD1-knockdown cells. A lentivirus-based vector expressing shRNA-resistant human NeuroD1 cDNA, but not control vector, suppressed Slit2 expression in NeuroD1-knockdown cells. C, E-boxes in the promoter region of the *Slit2* gene. There are 6 E-boxes (1–6) in the promoter region. ChIP 1–3, the primer location for the ChIP assay. D, for primers for the E-boxes, the DNA fragment was coprecipitated with anti-NeuroD1 antibody. GAPDH, glyceraldehyde 3-phosphate dehydrogenase. * $P < 0.05$, ** $P < 0.01$ (Student's *t*-test).

expressing either control shRNA or NeuroD1 shRNA, into 129/SVJ WT mice. Because control shRNA-treated mice died from their tumors at approximately 4 weeks, the deadline was set at 3 weeks in this experiment. We found that tumor sphere cells expressing NeuroD1 shRNA showed significantly less tumorigenic ability (Fig. 6D).

High NeuroD1 expression is closely associated with poor prognosis of human NB

Finally, we considered whether the data obtained were relevant to the clinical features of human NB. To examine this, we utilized the data of the AMC cohort study (23) and analyzed the overall and relapse-free survival probabilities with regard to the expression levels of NeuroD1 (2 probes). As shown in Figure 7A and B, high NeuroD1 expression was closely associated with poor prognosis of human NB in both of the probes tested.

Furthermore, we stratified the samples by *MYCN* amplification and age because these are important prognosis factors for NB. With regard to the relationship between NeuroD1 expression and *MYCN* status on survival probability of patients, we could not draw a conclusion, probably because of the limited number of patients with amplified *MYCN* (data not shown). On the contrary, when we stratified the samples by age, we obtained a significant effect of the NeuroD1 expression on survival of patients older than 1 year with one probe (206282_at; Fig. 7C). For another probe (1556057_s_at), we observed the same tendency as noted for the first probe, although larger and more balanced samples are needed to obtain firm statistical results: the *P* values were 0.041, in

Published OnlineFirst February 24, 2011; DOI:10.1158/0008-5472.CAN-10-3524

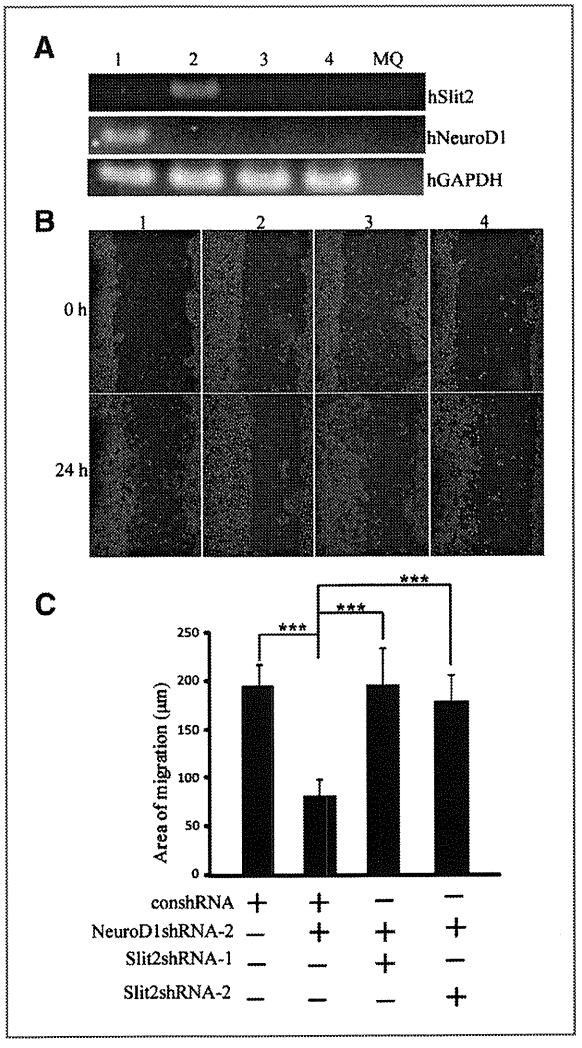

Figure 5. Slit2 knockdown restores the motility of NeuroD1-knockdown cells. Cells were treated with the following plasmids: 1, conshRNA plasmid; 2, conshRNA and NeuroD1 shRNA-2 plasmid; 3, NeruoD1 shRNA-2 and Slit2 shRNA-1 plasmid; 4, NeuroD1 shRNA-2 and Slit2 shRNA-2 plasmid. A, RT-PCR showing that NeuroD1-knockdown upregulates Slit2 (lane 2); this Slit2 expression is sufficiently suppressed by Slit2 shRNA (lanes 3 and 4). B and C, wound-healing assay data show that NeuroD1 knockdown inhibits cell motility whereas double knockdown of NeuroD1 and Slit2 restores the motility. ***, $P < 0.001$ (Student's t test). GAPDH, glyceraldehyde 3-phosphate dehydrogenase.

overall survival probability, and 0.063, in relapse-free survival probability (Fig. 7D).

Discussion

In this study, we have demonstrated that NeuroD1 is highly expressed in the neuroblast hyperplastic region, which is hypothesized to be a precancerous lesion of NB, suggesting that NeuroD1 is involved in NB tumorigenesis. Evidence in support of this hypothesis includes the fact that NeuroD1 knockdown led to suppression of NB cell motility and NB tumor sphere growth. Consequently, NeuroD1 knockdown suppressed *in vivo* tumor growth derived from tumor sphere cells. Consistent with these data, high expression of NeuroD1 was closely associated with poor prognosis of NB patients. Taken together, our data suggest that NeuroD1 plays a critical role in NB tumorigenesis.

Our results concur with the report by Revet and colleagues that inhibition of cell proliferation and anchorage-independent growth of a NB cell line by the Phox2B downstream target Msx1 is accompanied by downregulation of NeuroD1 (14). However, they found no significant difference in NeuroD1 expressions in NB and ganglioneuroma (differentiated benign tumor); this finding does not necessarily fit in with our results. Therefore, further studies are needed for understanding the roles of NeuroD1, particularly in terms of neural differentiation and NB tumorigenesis. In this context, it may be important to discuss the stemness of the neural progenitors and NB cells. NeuroD1 is expressed in proliferating neuronal progenitor cells not only during embryogenesis but also during adult neurogenesis. Its loss leads to a reduction in the number of differentiated neurons, such as cerebellar granule cells, the dentate gyrus cells, inner ear sensory neurons, amacrine cells, and newborn neurons in the adult hippocampus and olfactory bulb (4–10). In adult neurogenesis, the Wnt pathway activates β-catenin, which accumulates in the nucleus where it forms an activating complex with T-cell factor/lymphoid enhancer factor (TCF/LEF). The complex binds to the Sox/LEF element located in the promoter region of the *NeuroD1* gene and activates the transcription of NeuroD1. Thereafter, the neurogenesis process begins in the neural progenitor cells (9, 10). NeuroD1 may preserve the stemness of the neural progenitor cells, that is, it may promote self-renewal and differentiation. Furthermore, our findings showing its involvement in NB tumorigenesis support this idea. Interestingly, NeuroD1 was heterogeneously expressed, that is, it was not expressed in all the cells, and it was expressed in hyperplastic regions of 2-week-old *MYCN* Tg mice and NB tumors of *MYCN* Tg mice. Furthermore, NeuroD1 knockdown led to growth suppression of tumor spheres and *in vivo* tumors derived from tumor sphere cells. Considering that tumor-initiating cells are enriched in tumor spheres (24), it is conceivable that NeuroD1 is involved in the stemness property of NB cells. In line with this idea, NeuroD1 expression was induced in hyperplatic regions of *MYCN* Tg mice during the first 2 weeks after birth, thus suggesting that dynamic molecular events occur in these regions and lead to NB development.

Slit proteins (Slit1–Slit3) are secreted as extracellular matrix-associated glycoproteins and function as ligands for the repulsive guidance receptor Roundabout (Robo1–Robo4) family. Slit2 is known to bind with the Robo 1 receptor and regulates the migration of neurons during development (25). In the present study, we found that NeuroD1 downregulated Slit2 expression and promoted cell motility whereas NeuroD1 knockdown upregulated Slit2 expression and inhibited cell motility. This is the first study to illustrate an inverse relationship between NeuroD1 and Slit2. Significantly, Slit2 knockdown in NeuroD1-knockdown cells restored cell motility.

Published OnlineFirst February 24, 2011; DOI:10.1158/0008-5472.CAN-10-3524

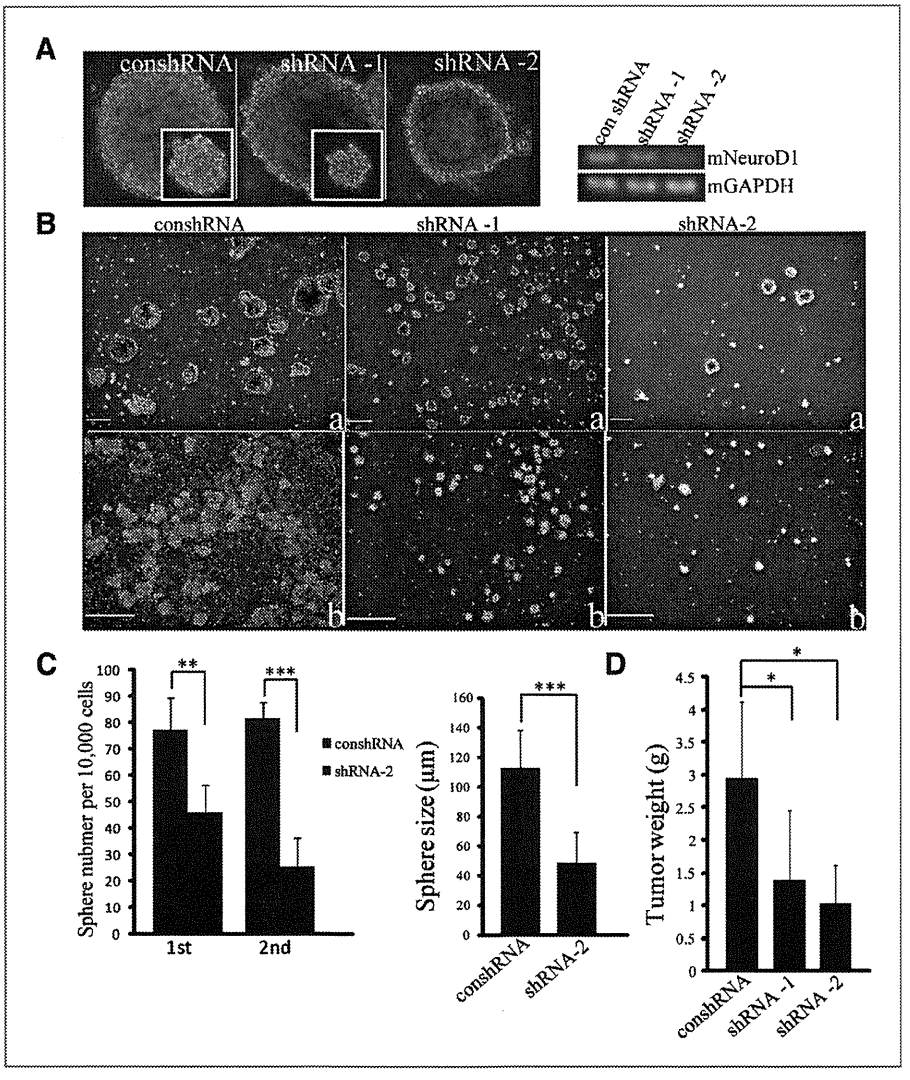

Figure 6. NeruoD1 knockdown suppresses tumor sphere growth and tumor growth. A, tumor sphere cells derived from NB tumors of *MYCN* Tg mice were infected with lentivirus expressing shRNA (photographs were taken 4 days after virus infection). RT-PCR shows efficient knockdown of NeuroD1expression by shRNAs. B, tumor sphere cells were completely dissociated into single cells by trypsin treatment and were infected with lentivirus expressing NeuroD1 shRNA or control shRNA. Cells were then cultured for 4 days (images indicated by an "a"). Cells were dissociated again and were further cultured for 4 days (images indicated by a "b") to form tumor spheres so that the ability of sphere formation and sphere growth could be evaluated. C, self-renewal ability of tumor spheres. An equal number (1×10^4) of sphere cells were cultured for 4 days, and the sphere number was counted for each generation. Furthermore, sphere size is shown for the first generation. The results for the second generation were similar (data not shown). D, an equal number (1×10^4) of control or NeuroD1 shRNA-infected sphere cells were subcutaneously injected into 129/SVJ WT mice ($n = 5$ for conshRNA and shRNA-1 treated group, $n = 2$ for shRNA-2 treated group). The tumors generated were removed and weighed 18 days after inoculation. Scale bar, 200 μm. *, $P < 0.05$; **, $P < 0.01$; ***, $P < 0.001$ (Student's *t* test). GAPDH, glyceraldehyde 3-phosphate dehydrogenase.

Therefore, Slit2 is, at least partly, involved in the NeuroD1-mediated regulation of cell motility. Cell motility is closely linked to tumor invasion and metastasis. Indeed, in our allograft NB model, we can find metastasized small tumors in the ipsilateral axillary lymph nodes usually at approximately 4 weeks after sphere cell inoculation (data not shown). Evidence in support of our findings includes the fact that *Slit2* is considered a candidate tumor suppressor gene; it is frequently inactivated in various cancers due to hypermethylation of its promoter region and allelic loss. Slit2 has a close relationship with cell migration and growth in tumor development (26–29). However, we did not observe a significant relationship between Slit2 expression and NB patient survival (data not shown). This may suggest that Slit2 does not entirely account for the role of NeuroD1 in NB development, although it is an important player downstream from NeuroD1.

In summary, we found an inverse relationship between NeuroD1 and Slit2 expression. NeuroD1 promotes cell motility and growth of tumor spheres as well as *in vivo* tumor growth. NeuroD1-mediated cell motility is at least in part due to Slit2

Published OnlineFirst February 24, 2011; DOI:10.1158/0008-5472.CAN-10-3524

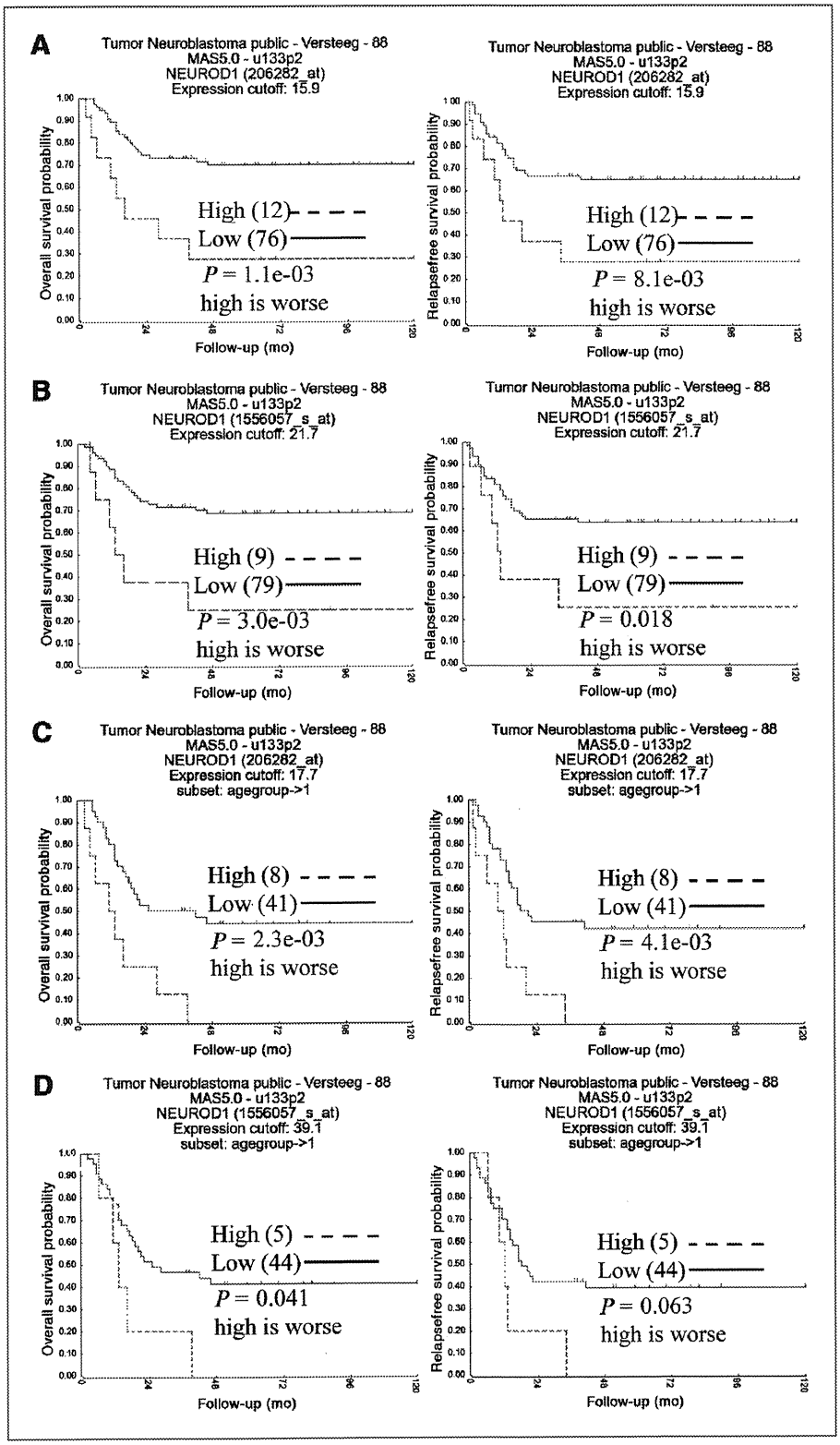

Figure 7. Kaplan–Meier analysis of the prognosis of NB patients in relation to NeruoD1 expression. A and B, Kaplan–Meier analysis of the AMC cohort ($n = 88$). Two probes (206282_at and 1556057_s_at) are available for NeuroD1 (A and B, respectively). C and D, effects of NeuroD1 on the survival of NB patients older than 1 year.

Published OnlineFirst February 24, 2011; DOI:10.1158/0008-5472.CAN-10-3524

suppression. Our findings highlight the close relation of early neurogenesis and NB tumorigenesis and provide candidate molecular targets for the development of NB therapy.

Disclosure of Potential Conflicts of Interest

No potential conflicts of interest were disclosed.

Acknowledgments

We thank Motoshi Suzuki (Nagoya University) for instruction us in FACS analysis, Didier Trono from the Swiss Federal Institute of Technology (EPFL, Switzerland) for providing the Lentivirus Packaging and Production plasmids psPAX2 and pMD2.G, and Hiroyuki Miyoshi from the Subteam for Manipulation of Cell Fate, RIKEN BioResource Center (Japan), and Atsushi Miyawaki from RIKEN Brain Science Institute (Japan) for providing the cDNA expression vector CSII-CMV-RfA-IRES2-Venus and control vector CSII-CMV-Venus. We also thank Tomoko Masuoka and Misako Tanase for their technical assistance.

Grant Support

This work was supported in part by a Grant-in-Aid for Cancer Research (20-13) from the Ministry of Health, Labour and Welfare, Japan, to K. Kadomatsu, by Grants-in-Aid (22790311 to S. Kishida; 21790317 to Y. Murakami-Tonami) from the Ministry of Education, Culture, Sports, Science, and Technology (MEXT), Japan, by a Grant-in-Aid from the Ministry of Agriculture, Forestry and Fisheries, Japan, to K. Kadomatsu and A. Onishi, and by funds from the Global COE program of MEXT, Japan, to Nagoya University.

The costs of publication of this article were defrayed in part by the payment of page charges. This article must therefore be hereby marked *advertisement* in accordance with 18 U.S.C. Section 1734 solely to indicate this fact.

Received September 29, 2010; revised February 1, 2011; accepted February 7, 2011; published OnlineFirst February 24, 2011.

References

1. Naya FJ, Huang H-P, Qiu Y, Mutoh H, DeMayo FJ, Leiter AB, et al. Diabetes, defective pancreatic morphogenesis, and abnormal enteroendocrine differentiation in BETA2/NeuroD-deficient mice. Genes Dev 1997;11:2323–34.
2. Lee JE, Hollenberg SM, Snider L, Turner DL, Lipnick N, Weintraub H. Conversion of *Xenopus* ectoderm into neurons by NeuroD, a basic helix-loop-helix protein. Science 1995;268:836–44.
3. Miyata T, Maeda T, Lee JE. NeuroD is required for differentiation of the granule cells in the cerebellum and hippocampus. Genes Dev 1999;13:1647–52.
4. Schwab MH, Bartholomae A, Heimrich B, Feldmeyer D, Druffel-Augustin S, Goebbels S, et al. Neuronal basic helix-loop-helix proteins (NEX and BETA2/Neuro D) regulate terminal granule cell differentiation in the hippocampus. J Neurosci 2000;20:3714–24.
5. Kim WY, Fritzsch B, Serls A, Bakel LA, Huang EJ, Reichardt LF, et al. NeuroD-null mice are deaf due to a severe loss of the inner ear sensory neurons during development. Development 2001;128:417–26.
6. Liu M, Pereira FA, Price SD, Chu M-j, Shope C, Himes D, et al. Essential role of BETA2/NeuroD1 in development of the vestibular and auditory systems. Genes Dev 2000;14:2839–54.
7. Morrow EM, Furukawa T, Lee JE, Cepko CL. NeuroD regulates multiple functions in the developing neural retina in rodent. Development 1999;126:23–36.
8. Kuwabara T, Hsieh J, Muotri A, Yeo G, Warashina M, Lie DC, et al. Wnt-mediated activation of NeuroD1 and retro-elements during adult neurogenesis. Nat Neurosci 2009;12:1097–105.
9. Gao Z, Ure K, Ables JL, Lagace DC, Nave K-A, Goebbels S, et al. Neurod1 is essential for the survival and maturation of adult-born neurons. Nat Neurosci 2009;12:1090–2.
10. Nakagawara A, Ohira M. Comprehensive genomics linking between neural development and cancer: neuroblastoma as a model. Cancer Lett 2004;204:213–24.
11. Howard MJ. Mechanisms and perspectives on differentiation of autonomic neurons. Dev Biol 2005;277:271–86.
12. Raabe EH, Laudenslager M, Winter C, Wasserman N, Cole K, LaQuaglia M, et al. Prevalence and functional consequence of PHOX2B mutations in neuroblastoma. Oncogene 2007;27:469–76.
13. Reiff T, Tsarovina K, Majdazari A, Schmidt M, del Pino I, Rohrer H. Neuroblastoma Phox2b variants stimulate proliferation and dedifferentiation of immature sympathetic neurons. J Neurosci 2010;30:905–15.
14. Revet I, Huizenga G, Chan A, Koster J, Volckmann R, van Sluis P, et al. The MSX1 homeobox transcription factor is a downstream target of PHOX2B and activates the Delta-Notch pathway in neuroblastoma. Exp Cell Res 2008;314:707–19.
15. Jögi A, Øra I, Nilsson H, Poellinger L, Axelson H, Påhlman S. Hypoxia-induced dedifferentiation in neuroblastoma cells. Cancer Lett 2003;197:145–50.
16. Brodeur GM. Neuroblastoma: biological insights into a clinical enigma. Nat Rev Cancer 2003;3:203–16.
17. Guillemot F, Lo L-C, Johnson JE, Auerbach A, Anderson DJ, Joyner AL. Mammalian achaete-scute homolog 1 is required for the early development of olfactory and autonomic neurons. Cell 1993;75:463–76.
18. Roybon L, Hjalt T, Stott S, Guillemot F, Li J-Y, Brundin P. Neurogenin2 directs granule neuroblast production and amplification while NeuroD1 specifies neuronal fate during hippocampal neurogenesis. PLoS One 2009;4:e4779.
19. Shida T, Furuya M, Kishimoto T, Nikaido T, Tanizawa T, Koda K, et al. The expression of NeuroD and mASH1 in the gastroenteropancreatic neuroendocrine tumors. Mod Pathol 2008;21:1363–70.
20. Weiss WA, Aldape K, Mohapatra G, Feuerstein BG, Bishop JM. Targeted expression of MYCN causes neuroblastoma in transgenic mice. EMBO J 1997;16:2985–95.
21. Hansford LM, Thomas WD, Keating JM, Burkhart CA, Peaston AE, Norris MD, et al. Mechanisms of embryonal tumor initiation: distinct roles for MycN expression and MYCN amplification. Proc Natl Acad Sci U S A 2004;101:12664–9.
22. Naya FJ, Stellrecht CM, Tsai MJ. Tissue-specific regulation of the insulin gene by a novel basic helix-loop-helix transcription factor. Genes Dev 1995;9:1009–19.
23. Huang S, Laoukili J, Epping MT, Koster J, Hölzel M, Westerman BA, et al. ZNF423 is critically required for retinoic acid-induced differentiation and is a marker of neuroblastoma outcome. Cancer Cell 2009;15:328–40.
24. Hansford LM, McKee AE, Zhang L, George RE, Gerstle JT, Thorner PS, et al. Neuroblastoma cells isolated from bone marrow metastases contain a naturally enriched tumor-initiating cell. Cancer Res 2007;67:11234–43.
25. Wong K, Ren X-R, Huang Y-Z, Xie Y, Liu G, Saito H, et al. Signal transduction in neuronal migration: roles of GTPase activating proteins and the small GTPase Cdc42 in the Slit-Robo pathway. Cell 2001;107:209–21.
26. Prasad A, Paruchuri V, Preet A, Latif F, Ganju RK. Slit-2 induces a tumor-suppressive effect by regulating β-catenin in breast cancer cells. J Biol Chem 2008;283:26624–33.
27. Tseng R-C, Lee S-H, Hsu H-S, Chen B-H, Tsai W-C, Tzao C, et al. Slit2 attenuation during lung cancer progression deregulates {beta}-catenin and e-cadherin and associates with poor prognosis. Cancer Res 2010;70:543–51.
28. Mertsch S, Schmitz N, Jeibmann A, Geng J-G, Paulus W, Senner V. Slit2 involvement in glioma cell migration is mediated by Robo1 receptor. J Neurooncol 2008;87:1–7.
29. Kim HK, Zhang H, Li H, Wu T-T, Swisher S, He D, et al. Slit2 inhibits growth and metastasis of fibrosarcoma and squamous cell carcinoma. Neoplasia 2008;10:1411–20.

Development/Plasticity/Repair

Keratan Sulfate Restricts Neural Plasticity after Spinal Cord Injury

Shiro Imagama,[1,2]* Kazuma Sakamoto,[1]* Ryoji Tauchi,[2] Ryuichi Shinjo,[2] Tomohiro Ohgomori,[1] Zenya Ito,[1,2] Haoqian Zhang,[1,3] Yoshihiro Nishida,[2] Nagamasa Asami,[4] Sawako Takeshita,[4] Nobuo Sugiura,[5] Hideto Watanabe,[5] Toshihide Yamashita,[6] Naoki Ishiguro,[2] Yukihiro Matsuyama,[2,7] and Kenji Kadomatsu[1]

Departments of [1]Biochemistry and [2]Orthopedics, Nagoya University Graduate School of Medicine, Showa-ku, Nagoya 466-8550, Japan, [3]Department of Neurosurgery, University of California, San Francisco, California 94143-0110, [4]Central Research Laboratories, Seikagaku Corporation, Higashiyamato, Tokyo 207-0021, Japan, [5]Institute for Molecular Science of Medicine, Aichi Medical University, Yazako, Nagakute, Aichi 480-1195, Japan, [6]Department of Molecular Neuroscience, Graduate School of Medicine, Osaka University, Suita, Osaka 565-0871, Japan, and [7]Department of Orthopedics, Hamamatsu University School of Medicine, Hamamatsu 431-3192, Japan

Chondroitin sulfate (CS) proteoglycans are strong inhibitors of structural rearrangement after injuries of the adult CNS. In addition to CS chains, keratan sulfate (KS) chains are also covalently attached to some proteoglycans. CS and KS sometimes share the same core protein, but exist as independent sugar chains. However, the biological significance of KS remains elusive. Here, we addressed the question of whether KS is involved in plasticity after spinal cord injury. Keratanase II (K-II) specifically degraded KS, i.e., not CS, *in vivo*. This enzyme digestion promoted the recovery of motor and sensory function after spinal cord injury in rats. Consistent with this, axonal regeneration/sprouting was enhanced in K-II-treated rats. K-II and the CS-degrading enzyme chondroitinase ABC exerted comparable effects *in vivo* and *in vitro*. However, these two enzymes worked neither additively nor synergistically. These data and further *in vitro* studies involving artificial proteoglycans (KS/CS-albumin) and heat-denatured or reduced/alkylated proteoglycans suggested that all three components of the proteoglycan moiety, i.e., the core protein, CS chains, and KS chains, were required for the inhibitory activity of proteoglycans. We conclude that KS is essential for, and has an impact comparable to that of CS on, postinjury plasticity. Our study also established that KS and CS are independent requirements for the proteoglycan-mediated inhibition of axonal regeneration/sprouting.

Introduction

The CNS extracellular matrix (ECM) may play a role in the maintenance of the neuronal network by inhibiting axonal growth and suppressing the formation of additional inadequate synapses. Upon neuronal injury, disorganized production of proteoglycans in the ECM is initiated, leading to the inhibition of structural rearrangement of the neuronal network. Among proteoglycans, chondroitin sulfate proteoglycans (CSPGs) have received particular attention; dystrophic end balls end in the CSPG deposition area at the injury site (Davies et al., 1999; Grimpe and Silver, 2004; Silver and Miller, 2004; Tom et al., 2004), and CSPGs inhibit neurite outgrowth *in vitro*. The chondroitin sulfate (CS)-degrading enzyme chondroitinase ABC (C-ABC) promotes axonal regeneration after nigrostriatal tract transaction (Moon et al., 2001), collateral sprouting of spared fibers in the cuneate nucleus after cervical spinal cord injury (SCI) (Massey et al., 2006), and functional recovery after SCI (Bradbury et al., 2002). Thus, the CS chains of the CSPG moiety seem to be principal for the CSPG-mediated inhibition of structural rearrangement.

Proteoglycans consist of a core protein and covalently attached long sugar chains of repeating disaccharide units with sulfation, or so-called glycosaminoglycans (GAGs). Four sulfated glycosaminoglycans are known, i.e., CS, dermatan sulfate, heparan sulfate, and keratan sulfate (KS). Most proteoglycans carry a single glycosaminoglycan (such as a CSPG or KSPG), but a few proteoglycans, e.g., aggrecan (KS/CSPG), have two types of glycosaminoglycan.

KS is expressed in the rodent roof plate of the spinal cord, and is induced after SCI and injury in the brain (Snow et al., 1990a; Cole and McCabe, 1991; Geisert et al., 1996; Jones and Tuszynski, 2002; Krautstrunk et al., 2002; Moon et al., 2002). *In vitro* digestion of KS restores neurite outgrowth on proteoglycan-coated substratum (Snow et al., 1990b; Powell et al., 1997). Thus, KS has been implicated in the regulation of axon guidance and/or axonal regeneration/sprouting. However, its biological impact on neu-

Received Sept. 29, 2010; revised Sept. 6, 2011; accepted Oct. 1, 2011.

Author contributions: S.I., H.Z., Y.N., N.A., S.T., N.S., H.W., T.Y., N.I., Y.M., and K.K. designed research; S.I., K.S., R.T., and R.S. performed research; S.I., T.O., Z.I., and K.K. analyzed data; S.I. wrote the paper.

This work was supported in part by a Grant-in-Aid for Scientific Research on Innovative Areas (No. 23110002 to K.K.) from Ministry of Education, Culture, Sports, Science, and Technology (MEXT), Japan; by Grants-in-Aid for Scientific Research (Nos. 18390099 and 20390092 to K.K.) from MEXT, Japan; by the Ministry of Health, Labor, and Welfare of Japan (Health Sciences Research Grant on Comprehensive Research on Disability Health and Welfare, H21-012 to K.K.); and by funds from the Global Centers of Excellence program, MEXT, Japan, to Nagoya University. We thank K. Suzuki, Y. Kurahashi, and A. Tanaka (Seikagaku Corporation) for performing the stability test of K-II and the HPLC analysis of sugar, M. Sawada (Nagoya University) for guidance with the primary culture of neurons, and N. Ozaki (Nagoya University) for guidance with the sensory tests. We also thank T. Natori (Yamanashi-Gakuin University) and M. Iida, Y. Naito, S. Nakashima, N. Misawa, and Y. Miwa (Nagoya University) for their excellent technical assistance.

*S.I. and K.S. contributed equally to this work.

Correspondence should be addressed to Kenji Kadomatsu, Department of Biochemistry, Nagoya University Graduate School of Medicine, 65 Tsurumai-cho, Showa-ku, Nagoya 466-8550, Japan. E-mail: kkadoma@med.nagoya-u.ac.jp.

DOI:10.1523/JNEUROSCI.5120-10.2011

 0270-6474/11/3117091-12$15.00/0

ronal injuries and the underlying mechanisms have been poorly studied. We have recently found that mice deficient in the enzyme *N*-acetylglucosamine 6-*O*-sulfotransferase-1 lose reactivity to the anti-KS antibody 5D4 in the brain, and show better axonal growth than wild-type mice after a cortical stab wound (Zhang et al., 2006). We have also found that the mice deficient in this enzyme show better motor function recovery and enhanced axonal regeneration/sprouting after SCI (Ito et al., 2010). However, as these knock-out mice lose *N*-acetylglucosamine 6-*O*-sulfotransferase-1 in every cell in the body, critical questions remain to be answered, e.g., whether KS specifically works in the spinal cord, and how much impact KS has on functional disturbance. Furthermore, with regard to the functional redundancy between CS and KS, it is also an important question whether KS collaborates with CS, or works independently.

In the present study, we used keratanase II (K-II), which specifically degrades KS, and investigated the role of KS in postinjury plasticity. We found that KS and CS have a comparable impact on this form of plasticity. We also determined the structural basis of proteoglycan-mediated inhibition of neural plasticity.

Materials and Methods

Surgical procedure. Adult female Sprague Dawley rats weighing 200–230 g were used in the study of SCI. The animals were anesthetized with an intraperitoneal injection of ketamine (100 mg/kg) and xylazine (10 mg/kg). After Th9 laminectomy, we exposed the dura mater and induced injury using a force of 200 kdyn using a commercially available SCI device (Infinite Horizon Impactor; Precision Systems and Instrumentation) that provided a consistent degree of spinal cord contusion injury. All injuries included the dorsal CST and dorsal gray matter. Immediately after the spinal cord contusion, we performed a Th12 partial laminectomy, inserted a thin silicone tube with an osmotic mini-pump into the subarachnoid cavity, and set the tube tip at the Th9 level under a surgical microscope. This tube was very soft and thin so that we could minimize damage to the spinal cord. The osmotic mini-pumps (200 μl of solution, 0.5 μl/h, 14 d delivery; Alzet pump model 2002 [Durect]) were filled with K-II (0.05 U/200 μl; purified from *Bacillus circulans*) (Yamagishi et al., 2003), C-ABC (0.05 U/200 μl) (Seikagaku), or saline (as a vehicle control). To determine an appropriate dose of C-ABC, we examined several doses and found that at the doses of 0.05, 0.1, and 1.0 U/200 μl, C-ABC showed a comparable effect on motor function recovery, while the dose of 0.025 U/200 μl showed a less potent effect (supplemental Fig. 1, available at www.jneurosci.org as supplemental material). Therefore, we used 0.05 U/200 μl of C-ABC in this study.

The tube was sutured to the spinous process to anchor it in place, and the mini-pump was placed under the skin on the animal's back. Afterward, the muscles and skin were closed in layers. The bladder was compressed by manual abdominal pressure twice a day until bladder function was restored. Food was provided on the cage floor, and the rats had no difficulty reaching their water bottles. All animals were given antibiotics in their drinking water [1.0 ml of Bactramin (Roche) in 500 ml of acidified water] for 2 weeks after SCI. We excluded the rats without complete paraplegia on the next day after operation in all groups as they were inappropriate for further evaluation. Although the number of such rats was very small (~1 of 70 rats after injury with our hands), we consistently found that rats without complete paraplegia showed a histology of incomplete injury of the spinal cord. However, no rats were excluded from any groups thereafter, with the exception of rats that had died. We performed postmortem histological measurement and found that all the dead rats had complete severe injury in the spinal cord (data not shown). Therefore, it was not likely that rats with serious spinal shock but minor injury were involved in the experiments in the current study. The number of rats undergoing operation and the number of rats evaluated in each experiment are summarized in Table 1. All animals were treated and cared for in accordance with the Nagoya University School of Medicine Guidelines pertaining to the treatment of experimental animals.

Basso, Beattie, and Bresnahan open field locomotor test. The recovery of hindlimb motor function was assessed by determining the Basso, Beattie, and Bresnahan (BBB) scores (Basso et al., 1995). The results were quantified in a blinded manner by two observers.

Table 1. Number of rats undergoing operation and evaluated in each experiment

Models	Rats	
	Number used for operation	Final number evaluated
EXP1: concentration (Fig. 2*D*,*E*)		
K-II 0.05 U	10	7
K-II 0.005 U (1/10)	10	5
K-II 0.000025 U (1/2000)	10	6
K-II (heat-denatured)	10	5
Vehicle	10	7
EXP2: functional recovery (Fig. 2*A*,*B*)		
K-II 0.05 U	12	10
C-ABC	12	7
Vehicle	12	10
EXP3: functional recovery (Fig. 2*F*)		
Vehicle	12	9
C-ABC	12	7
K-II	12	11
K-II + C-ABC	12	7
EXP4: MEP (Fig. 2*C*)		
Sham	10	8
Vehicle	10	9
C-ABC	10	5
K-II	10	7
K-II + C-ABC	10	7

EXP, Experiment.

%Grip test. Paw placement for each limb on the grid bar was assessed as the animal walked on a plastic-coated wire mesh grid (50 cm length × 33 cm width × 20 cm height, with 2.5 × 2.5 cm openings) for 3 min. Steps in which the paw gripped the grid bar and supported the animal's weight were counted as correct. The number of correct paw placements was expressed as a percentage of the total steps. The percentage of correct paw placements was calculated for each hindlimb and averaged.

Touch test. A touch test was performed preoperatively and then weekly after the operation. Rats were habituated for 30 min in elevated clear plastic cages with wire mesh grid floors. Graded von Frey hair (vFH) monofilaments were applied to the plantar surface of the foot, ~1 cm posterior to the footpad of the middle phalange with the up-down method using procedures described in detail previously (Hutchinson et al., 2004).

Testing began with 15.14 g vFH applied to the hindpaw and continued until 10 trials per hindpaw were completed. Rats were given a food reward throughout testing to prevent visual recognition of the application of the monofilament. A trial was discarded and reperformed if vFH application lifted the paw, producing proprioceptive rather than tactile input. A positive response occurred when the paw was briskly withdrawn from the monofilament. The lowest gram force that produced withdrawal was designated as the response threshold. The thresholds of the bilateral hindpaws were averaged. It was previously determined that the average vFH hindpaw threshold in normal rats is 60 g; in the present study, therefore, we preoperatively excluded rats with a vFH threshold higher than this value. The examiners were blind to group assignment during the vFH testing.

Tail-immersion test. The tail-immersion test was used to determine the somatic thermo-threshold of rats preoperatively and then weekly after the operation. Briefly, rats were gently lifted from their home cages and taken to the test room, where the withdrawal latency of the tail to a temperature stimulus was measured by immersing the tail in a 55 ± 0.5°C water bath. The cutoff time was set at 8 s to avoid skin damage. Rats underwent this test three times at intervals of 15 min. The measurements were averaged to obtain the withdrawal latency time in seconds. Between sessions, the rats were returned to their home cages. Based on the results, we preoperatively excluded rats with prolonged withdrawal latency. Examiners were blind to the group assignment during the tail-immersion test.

Western blotting. The 10-mm-long sections of the injured spinal cord at 1 week after SCI were dissected and homogenized in PBS including 1%

Table 2. Purification of keratanase II

Step	Enzyme activity (units)		
	BcKeratanase	Chondroitinase	α-Galactosidase
Cell extract	38.000	7.000	12.000
Salting out	33.060	3.500	3.960
Desalting	29.260	3.150	3.600
DEAE-cellulose	20.900	0.013	2.400
Phenyl-sepharose	20.900	0.000	0.000

Keratanase unit: One unit will liberate 1.0 μmol of reducing sugar as 2-acetamido-2- deoxy-D-glucose from keratan sulfate per minute at pH 6.0 at 37°C. Chondroitinase unit: One unit will liberate 1.0 μmol of 2-acetamido-2-deoxy-3-*O*-(β-D-gluc-4-ene-pyranosyluronic acid)-6-*O*-sulfo-D-galactose from chondroitin sulfate C per minute at pH 8.0 at 37°C. α-Galactosidase unit: One unit will hydrolyze 1.0 μmol of *p*-nitrophenyl-α-D-galactopyranoside per minute at pH 6.5 at 37°C.

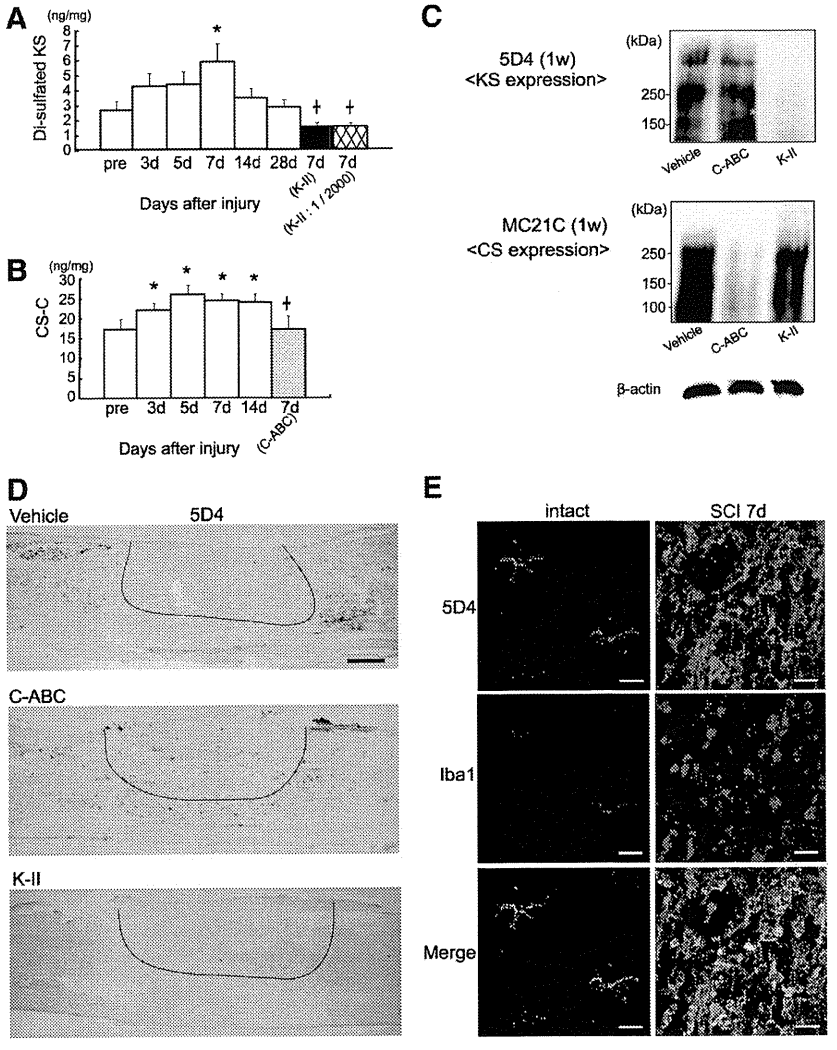

Figure 1. Specific degradation of KS by K-II. ***A***, Amounts of disulfated KS after SCI. A 10 mm fragment of the injured spinal cord was subjected to the analysis. Data represent the means ± SEM. $^{*}p < 0.05$ versus the preinjured specimen (pre). $^{+}p < 0.05$ versus 7 d; $n = 5$ in each group. K-II, 0.05 U of K-II was administered to the spinal cord; K-II 1/2000, 0.0000025 U of K-II was administered to the spinal cord. ***B***, Amounts of CS-C after SCI. $^{*}p < 0.05$ versus pre; $^{+}p < 0.05$ versus 7 d; $n = 6$ in each group. C-ABC, 0.05 U of C-ABC was administered to the spinal cord. ***C***, Rats were treated with K-II or C-ABC for 1 week after spinal cord injury. A 10 mm specimen of the injured spinal cord was subjected to Western blot analysis for 5D4-reactive KS, MC21C-reactive CS, and β-actin. ***D***, 5D4-reactive KS was visible in the penumbra region in vehicle- and C-ABC-treated rats, but not in K-II-treated rats. These rats were treated with the indicated enzyme for 1 week after spinal cord injury. Scale bars, 500 μm. All photos are of sagittal sections with the left side rostral. ***E***, Double staining for KS (5D4) and microglia (Iba1). The left panels show the intact spinal cord, and the right panels show the spinal cord 1 week after injury. Most 5D4-reactive cells overlapped Iba1-positive cells, which indicated that KS was mainly expressed by microglia. The left images showed ramified microglia expressing 5D4-KSPG. The right images show that 5D4-KSPG expression is seen on characteristic cellular profiles with short processes and a less ramified morphology after SCI. Scale bars, 20 μm.

Triton X-100 and protease inhibitors solution (Sigma). Samples of the supernatant fraction were collected after centrifuging at 10,000 × *g* for 30 min. Thirty microliters of each sample was applied and separated by electrophoresis on 6% SDS-PAGE. Proteins were then blotted onto nitrocellulose membranes. Blots were blocked with 5% fat-free dry milk in PBS for 60 min and incubated overnight at 4°C with the primary antibody anti-KS 5D4 (1 μg/ml; Seikagaku) or anti-CS MC21C (1 μg/ml; Seikagaku) in PBS containing 0.3% Triton X-100, washed, and then incubated with a second antibody, HRP-conjugated goat anti-mouse IgM (1/5000; Southern Biotechnology), at room temperature for 60 min. Anti-β-actin antibody (1/100,000; Sigma) was also used as indicated. Bound antibodies were visualized with an ECL-plus Western blotting detection kit (GE Healthcare).

Immunohistochemistry and immunocytochemistry. After terminal anesthesia by ether hyperaspiration, rats were perfused transcardially with buffered 4% paraformaldehyde. The spinal cords and brains were removed, postfixed overnight, and then cryoprotected in buffered 30% sucrose the next night. Tissues were cut into 20 μm sections with a cryostat and mounted on glass slides. The sections were blocked in PBS containing 3% BSA and 5% normal mouse serum for staining of biotin-conjugated anti-KS 5D4 or blocked in PBS containing 1% BSA and 10% normal goat serum for other immunohistochemistry. The sections were then incubated with the primary antibodies to KS (5D4; Seikagaku), Iba1 (Wako Pure Chemical Industries), GAP-43 (Millipore), serotonin (5-HT, Immunostar), type IV collagen (LSL), and GFAP (Sigma). After rinsing, the sections were incubated with the secondary antibody for 60 min at room temperature: Cy3- or Cy2-conjugated streptavidin (Jackson ImmunoResearch), Cy3-conjugated goat anti-rabbit IgG (Zymed Laboratories), Cy3-conjugated goat anti-mouse IgM (Jackson ImmunoResearch), FITC-conjugated goat anti-rat IgG (Sigma), and Alexa Fluor 488 goat anti-mouse IgG (Invitrogen). Sections were then rinsed, mounted with FluorSave (Calbiochem), and examined by confocal microscopy (MRC 1024; Bio-Rad Laboratories).

Morphometry. The extent of axonal outgrowth of each wound area was assessed by counting signals visualized on staining with GAP-43 and 5-HT using serial sagittal 20 μm sections. Morphometry analysis was performed using a computer-driven microscope stage (MetaMorph Offline, version 6.3r^2; Molecular Devices Corporation). In all sagittal sections shown here, the left side is rostral.

Anterograde labeling of the corticospinal tract. Eight weeks after injury, descending corticospinal tract (CST) fibers were labeled with biotin-dextran amine (BDA; 10% in saline, 3.5 μl per cortex, molecular weight 10,000; Invitrogen) injected under anesthesia into the left and right motor cortices (coordinates, 2 mm posterior and 2 mm lateral to the bregma; 1.5 mm depth). For each injection, 0.25 μl of BDA was delivered for a period of 30 s via a 15–20 μm inner diameter glass capillary attached to a microliter syringe (ITO Corporation). Two weeks after BDA injection, the animals were killed by perfusion with PBS followed by 4% paraformaldehyde. The spinal cords were dissected, postfixed overnight in the same fixa-

tives, and cryopreserved in 30% sucrose in PBS. A 20 mm length of spinal cord, 10 mm rostral and 10 mm caudal to the lesioned site, was embedded in Tissue-Tek OCT. These blocks were sectioned in the transverse plane (25 μm). Sections were incubated in PBS with 0.3% Triton X for 4 h and then incubated for 2 h with Alexa Fluor 488-conjugated streptavidin (1:400; Invitrogen) in PBS with 0.05% Tween 20. We then took serial cross sections of the spinal cord and quantitatively analyzed the distribution of the axons. Degrees of BDA uptake were assessed by counting the total number of fibers in the cross section 10 mm rostral to the lesioned site, where the CST was intact. For quantification of the number of labeled corticospinal axons 10 mm caudal to the lesion site, the number of labeled fibers was counted in the gray matter, the dorsal CST area (normal locations of the dorsal CST), or the white matter except for the dorsal CST area, and divided by the number of labeled corticospinal axons 10 mm above the lesion. The labeled fibers were counted using MetaMorph software (Molecular Devices Corporation). Light intensity and thresholding values were maintained at constant levels for all analyses.

Motor-evoked potential. In terminal electrophysiological experiments, after an intraperitoneal injection of ketamine (100 mg/kg), short trains of five square-wave stimuli of 0.5 ms duration at interstimulus intervals of 2 ms were delivered through the epidural electrode catheter at a point 10 mm rostral from the epicenter. The active electrode was placed in the muscle belly, and the reference electrode was placed near the distal tendon of the muscle in each gastrocnemius. The ground electrode was placed subcutaneously between the epidural electrode and the recording electrodes. The onset latency was measured as the length of time in milliseconds between the stimulus and the onset of the first wave. The duration was also measured as the length of time in milliseconds between the waves. One hundred responses were averaged and stored for off-line analysis.

Spinal cord-evoked potential after stimulation to the spinal cord. For sensory assessment, we performed spinal cord-evoked potential after stimulation to the spinal cord (sp-SCEP), which recognized extrapyramidal pathways including dorsal column axons (Sutter et al., 2007; Tamaki and Kubota, 2007). Stimulations were delivered through the epidural electrode catheter at a point 10 mm caudal from the epicenter and measured at a point 10 mm rostral from the epicenter. The ground electrode was placed subcutaneously between the epidural electrodes. The onset latency and peak latency were measured as the length of time in milliseconds between the stimulus and the onset and the peak of the first wave, respectively. A total of 100 responses were averaged and stored for off-line analysis of the latency.

Measurement of CS and KS. After freeze-drying, each specimen was digested with 0.7 ml of 2.5% actinase E (Kaken Pharmaceutical Corporation) at 55°C for 24 h. The digest was then kept at 100°C for 5 min and centrifuged at 3000 rpm for 10 min. The CS concentration was determined according to the description of Shinmei et al. (1992) with some modifications. A 0.2 ml aliquot of the supernatant was digested with 250 mU of C-ABC (Seikagaku) and 25 mU of chondroitinase AC-II (Seikagaku) in 20 mM Tris-HCl buffer, pH 8, at 37°C for 2 h. The sample was ultrafiltrated using a Nanosep centrifugal device (molecular size cutoff 10,000; PALL), and the filtrate, which contained the unsaturated disaccharides Δdi-0S, Δdi-4S, and Δdi-6S derived from CS, was analyzed by HPLC.

The KS concentration was measured according to the method of Shinmei et al. (1992) with some modifications. A 0.15 ml aliquot of the supernatant was digested with 1 mU of K-II (Seikagaku) in 20 mM sodium acetate buffer, pH 6, at 37°C for 3 h. The sample was then ultrafiltrated using a Nanosep centrifugal device, and the filtrate, which contained the saturated disaccharides β-galactosyl-(1–4)-6-*O*-sulfo-*N*-acetylglucosamine and β-6-*O*-sulfogalactosyl-(1–4)-6-*O*-sulfo-*N*-acetylglucosamine derived from KS, was analyzed by HPLC.

The HPLC system used in this study consisted of a Model 2000 high-performance chromatograph (Jasco) and a stainless steel column packed

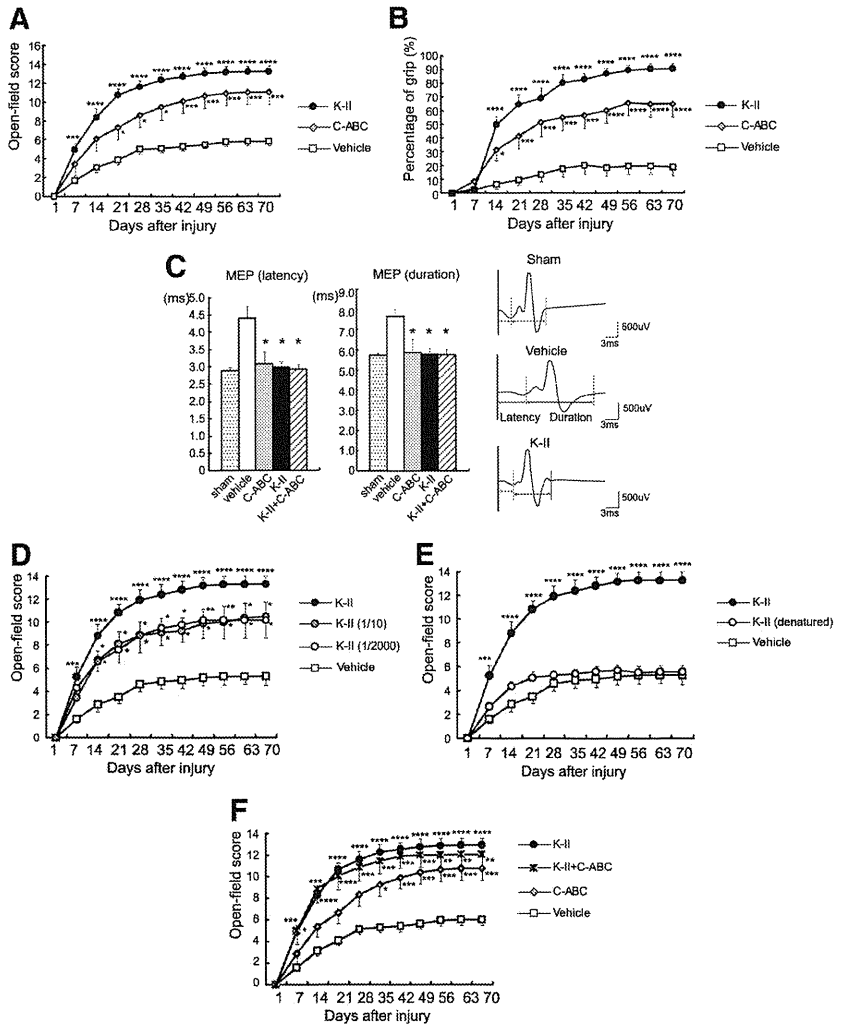

Figure 2. Motor function recovery by K-II after SCI. ***A***, ***B***, The BBB score and %grip test data after SCI. Recovery was significantly better in the K-II and C-ABC treatment groups than in the vehicle-administered control. Data represent the means ± SEM. $*p < 0.05$; $***p < 0.005$; $****p < 0.001$ versus the vehicle control ($n = 10$ K-II; $n = 7$ C-ABC; $n = 10$ Vehicle). ***C***, Electrophysiologic tests using MEP also showed functional recovery in the treatment groups at 8 weeks after SCI. Data represent the means ± SEM. $*p < 0.05$ versus the vehicle control ($n = 8$ Sham; $n = 9$ Vehicle; $n = 5$ C-ABC; $n = 7$ K-II; $n = 7$ K-II + C-ABC). ***D***, Motor function recovery after SCI in rats treated with K-II at various doses. K-II promoted functional recovery at a concentration of 0.05 U, and even restored motor function at concentrations of 0.005 U (1/10) and 0.0000025 U (1/2000). Data represent the means ± SEM. $*p < 0.05$; $**p < 0.01$; $***p < 0.005$; $****p < 0.001$ versus the vehicle control [$n = 7$ K-II; $n = 5$ K-II (1/10); $n = 6$ K-II (1/2000); $n = 7$ Vehicle]. ***E***, Heat-denatured K-II failed to promote motor function recovery after spinal cord injury. Data represent the means ± SEM. $***p < 0.005$; $****p < 0.001$ versus the vehicle control ($n = 7$ K-II; $n = 5$ Heat-denatured K-II; $n = 7$ Vehicle). ***F***, The combination of K-II and C-ABC did not show additive or synergistic effects on motor function (BBB score). Data represent the means ± SEM. $*p < 0.05$; $**p < 0.01$; $***p < 0.005$; $****p < 0.001$ versus the vehicle control ($n = 9$ Vehicle; $n = 7$ C-ABC; $n = 11$ K-II; $n = 7$ K-II + C-ABC).

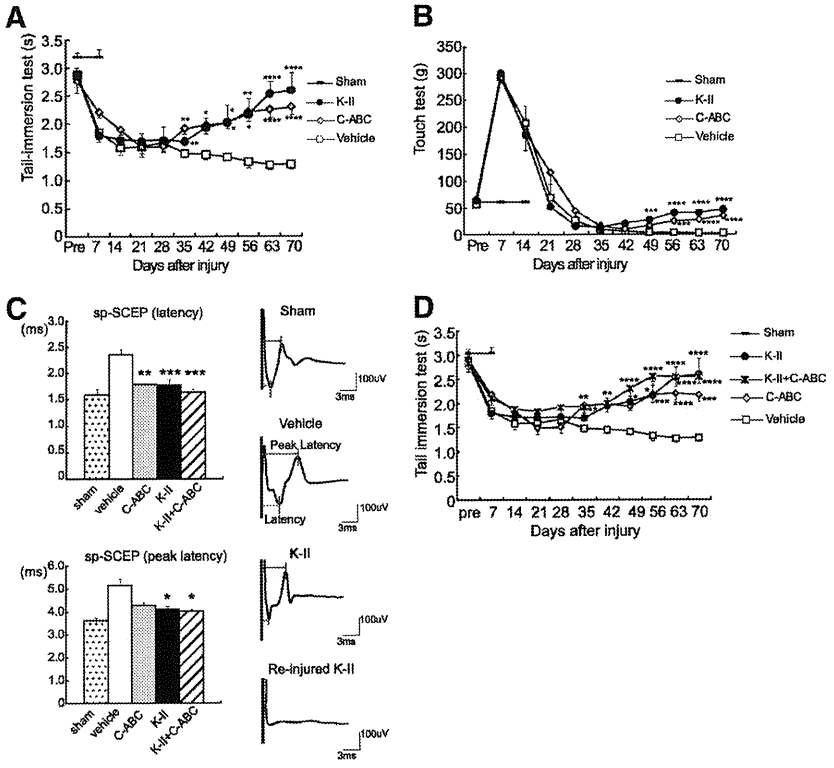

Figure 3. Sensory function recovery by K-II after SCI. ***A***, The tail-immersion test indicated that there was little allodynia in the K-II- and C-ABC-treated rats. Data represent the means ± SEM. $*p < 0.05$; $**p < 0.01$; $****p < 0.001$ versus the vehicle control ($n = 7$ Sham; $n = 5$ K-II; $n = 7$ C-ABC; $n = 9$ Vehicle). ***B***, The touch test also indicated that there was little allodynia in the K-II- and C-ABC-treated rats. Data represent the means ± SEM. $*p < 0.05$; $***p < 0.005$ versus the vehicle control ($n = 7$ Sham; $n = 5$ K-II; $n = 7$ C-ABC; $n = 9$ Vehicle). ***C***, Electrophysiologic tests using sp-SCEP showed not only motor functional recovery but also sensory recovery in the treatment groups at 8 weeks after SCI. The reinjury of K-II-treated rats lost the recovered response of sp-SCEP. Data represent the means ± SEM. $*p < 0.05$; $**p < 0.01$; $***p < 0.005$ versus the vehicle control ($n = 8$ Sham; $n = 7$ Vehicle; $n = 5$ C-ABC; $n = 6$ K-II; $n = 5$ K-II+C-ABC). ***D***, The combination of K-II and C-ABC did not show additive or synergistic effects on sensory function (tail-immersion test). Data represent the means ± SEM. $*p < 0.05$; $**p < 0.01$; $***p < 0.005$; $****p < 0.001$ versus the vehicle control ($n = 8$ Sham; $n = 9$ Vehicle; $n = 7$ C-ABC; $n = 11$ K-II; $n = 7$ K-II+C-ABC).

with polyamine-bound silica (YMC gel PA-120; YMC). The disaccharides in each sample were eluted with a gradient of 0–100 mM sodium sulfate. To the eluant from the column was added 100 mM sodium tetraborate buffer, pH 9, containing 1% 2-cyanoacetamide. The mixture was thermostated at 145°C, and the effluent was monitored by a fluoromonitor.

Cell culture. Sprague Dawley rats at postnatal days 7–9 were killed and their cerebella were collected. The meninges were carefully removed with fine forceps, and the tissues were minced and digested using a Papain Dissociation System (Worthington). Dissociated cells were applied to a 35/60% two-step Percoll gradient and centrifuged at 3000 × *g* for 15 min. Cerebellar granule neurons at the interface were collected. Cells were suspended in Neurobasal medium (Invitrogen) supplemented with 2% B27 (Invitrogen), 2 mM glutamine, an additional 20 mM KCl, 50 U/ml penicillin, and 50 μg/ml streptomycin.

Substrate preparation. Four-well chamber slides (Nunc) were coated with 20 μg/ml poly-L-lysine (PLL) (Sigma) and left overnight at 4°C. They were then coated with the indicated substrates and left for 4 h at 37°C. If indicated, proteoglycans or aggrecan were treated with 200 mU/ml C-ABC, 500 mU keratanase, and 5 mU/ml K-II derived from *Bacillus* sp. Ks36 or 5 mU endo-β-galactosidase (all from Seikagaku) in PBS at 37°C. Other substrate materials included poly-L-ornithine, aggrecan, and MAG (Sigma), Nogo and OMgp (R&D Systems), and KS and CS-C (Seikagaku).

Neurite outgrowth assay. Cerebellar granule neurons were seeded onto four-well chamber slides at 2.0×10^5/well. Twenty-four hours after seeding, the neurons were fixed with 4% paraformaldehyde/PBS and stained with anti-neuron-specific β-tubulin (Covance) to visualize the neurites. Neurite lengths were measured from at least 100 neurons per condition from duplicate wells, and quantified as described previously (Sivasankaran et al., 2004).

For reducing/alkylating proteoglycans, 5 μg of proteoglycans were suspended in 10 ml of 50 mM ammonium bicarbonate/PBS and reduced with 20 mM DTT for 60 min at 37°C. Then proteoglycans were alkylated with 10 mM iodoacetamide for 30 min at room temperature under dark condition. The proteoglycan solution was dialyzed against PBS for overnight and subjected to neurite outgrowth assay.

Preparation of GAG-BSA. CS-BSA was prepared as reported previously (Pumphrey et al., 2002) with minor modifications. Briefly, 20 mg of CS and 13 mg of BSA were linked using $NaBH_3CN$. CS-BSA was purified using anion-exchange chromatography (Q-Sepharose; GE Healthcare) followed by gel-filtration chromatography (Superose6 HR10/300; GE Healthcare) to remove free-BSA and free-CS, respectively. The protein concentration and KS concentration were quantified using a BCA Protein Assay Kit (Pierce) and HPLC analysis, respectively.

Because KS had an oligopeptide at its reducing end, we performed cross-linking between this peptide and BSA. Briefly, amino residues of this peptide were succinylated to inhibit self-cross-linking. Fifty-two milligrams of BSA and 20 mg of succinylated KS were cross-linked using *N*-hydroxysuccinimide (Pierce) and 1-ethyl-3-[3-dimethylaminopropyl]carbodiimide hydrochloride (Pierce). KS-BSA was purified using anion-exchange chromatography (Q-Sepharose; GE Healthcare) followed by gel-filtration chromatography (Superose6 HR10/300; GE Healthcare) to remove free-BSA and free-KS, respectively. The protein concentration and KS concentration were quantified using a BCA Protein Assay Kit (Pierce) and a Sulfated Glycosaminoglycan Quantification Kit (Seikagaku), respectively.

CS/KS-BSA was prepared by linking KS to CS-BSA.

Statistical analysis. We performed statistical analysis with an unpaired two-tailed Student's *t* test for single comparisons and one-way ANOVA for multiple comparisons. For the BBB score, %grip test, touch test, and tail-immersion test, we used repeated-measures ANOVA and Tukey's test. In all statistical analyses, significance was accepted at $p < 0.05$.

Results

In vitro and *in vivo* degradation of KS by K-II

We purified K-II from *B. circulans* as previously described (Yamagishi et al., 2003). Although the extracts of *B. circulans* showed both keratanase and chondroitinase activities, our stepwise protocol completely abolished the chondroitinase activity and purified K-II (Table 2). Furthermore, it is known that the purified enzyme does not digest hyaluronic acid, heparan sulfate, or heparin (Yamagishi et al., 2003). This enzyme is thermo-stable; indeed, it retained its enzymatic activity for at least 120 h at 37°C (100 ± 1.606% at 0 h vs 91.9 ± 4.014% at 120 h). Therefore, we decided to use this enzyme for *in vivo* experiments.

We asked whether K-II worked *in vivo*. To this end, we inflicted contusion injuries using a force of 200 kdyn in the rat spinal cord at the ninth thoracic vertebral level. This contusion model completely destroyed the dorsal columns and dorsal CST

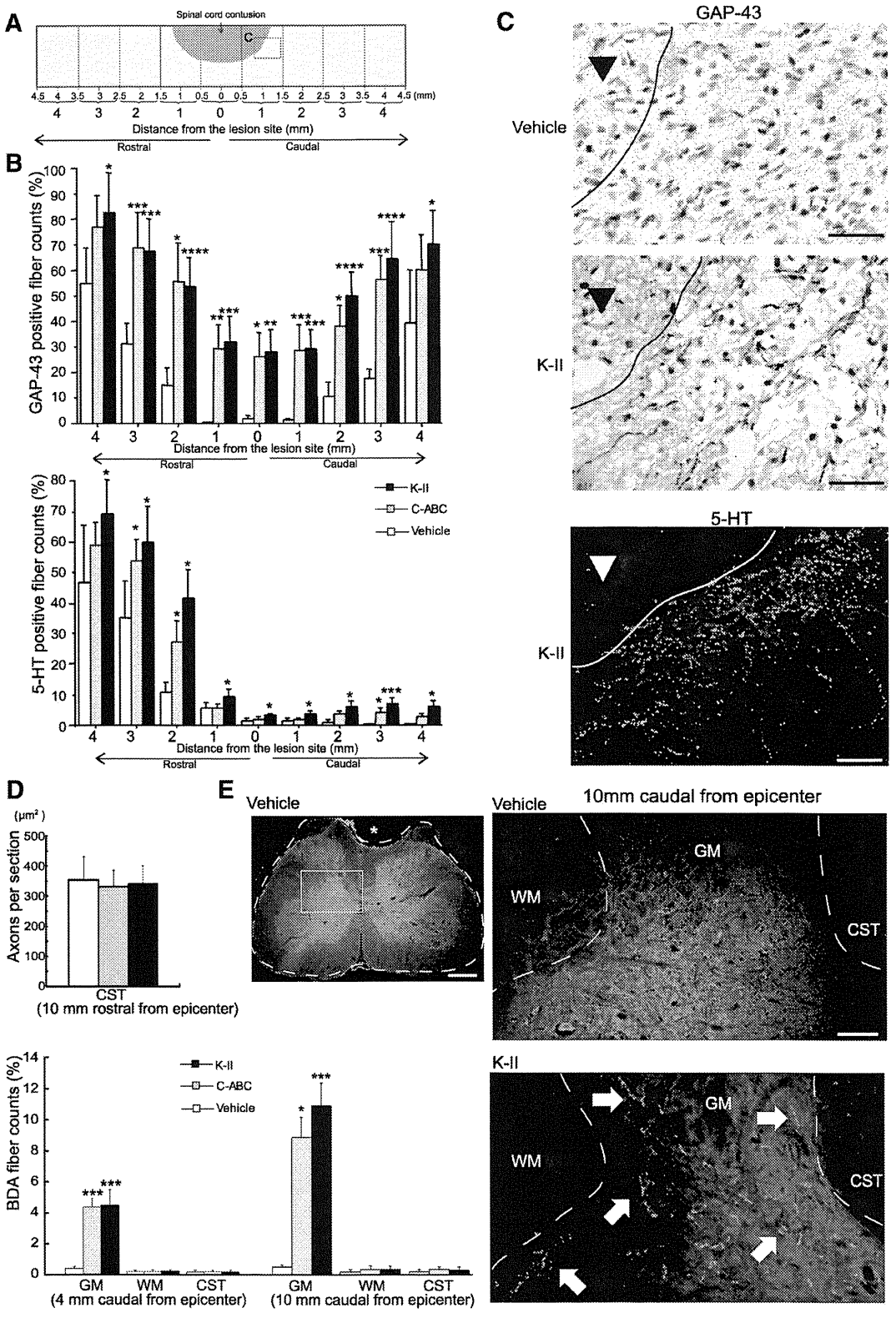

Figure 4. Histological analysis. ***A***, The scheme of the methods to reconstruct serial sagittal sections. On each section, the number of GAP-43- and 5-HT-positive fibers was counted from 4 mm rostral to 4 mm caudal the lesion site. The number was calculated as a percentage of the fibers seen in the sham-operated spinal cord. All serial sections were evaluated at 10 weeks after SCI. ***B***, Reconstruction of serial parasagittal section of the number of GAP-43- and 5-HT-positive fibers, represented as a percentage of the fibers seen in the sham-operated spinal cord. Data represent the means ± SEM. $*p < 0.05$; $**p < 0.01$; $***p < 0.005$; $****p < 0.001$ versus the vehicle control ($n = 5$ Vehicle; $n = 5$ C-ABC; $n = 6$ K-II). ***C***, Immunohistochemical analysis of GAP-43 and 5-HT (serotonin) expression in the injured spinal cord of the boxed area in scheme ***A*** at 10 weeks after SCI. Scale bars, 50 μm for the panels of GAP-43; 100 μm for the panel of 5-HT. All images are of sagittal section with the left side rostral. Arrowheads indicate the contusion area. ***D***, BDA labeling of CST. The top graph represents the number of labeled corticospinal (*Figure legend continues.*)

in the spinal cord. The injury was so severe that the lesion core, which was filled with collagen IV 1 week after injury, occupied a significant area of the spinal cord (data not shown). The injury sizes estimated by collagen IV or GFAP staining did not vary between individual rats (data not shown).

Disulfated KS contents in the injured region increased after injury, peaking at 7 d (Fig. 1*A*). CS-C contents also increased, peaking at ~7 d after injury (Fig. 1*B*), consistent with a previous report (Properzi et al., 2005).

K-II (0.05 U) or C-ABC (0.05 U) was then locally administered to the injured site for 2 weeks after contusion injuries using an osmotic pump. Disulfated KS contents decreased to the non-injury level after K-II treatment (Fig. 1*A*). Western blot and immunohistochemical analyses revealed that the reactivity to KS antibody 5D4 was lost in rats treated with K-II for 7 d after injury, but not in C-ABC-treated rats (Fig. 1*C*,*D*). The smear appearance in Western blot is probably due to the long sugar chains, and is the nature of proteoglycans. The granular staining profile in Figure 1*D* represented the main source of KS expression, i.e., microglia (Fig. 1*E*), which is consistent with previous reports (Jones and Tuszynski, 2002; Ito et al., 2010). As disulfated KS was still detected after K-II treatment by disaccharide analysis using HPLC (Fig. 1*B*), the almost complete disappearance of KS in Western blot and immunohistochemistry may be due to the limited ability of the 5D4 antibody to detect KS.

To detect diffusion of infused enzyme, biotin-labeled K-II was infused and detected by immunohistochemistry. We found that the enzyme diffused to cover the most area of injury, but did not cover the whole spinal cord (supplemental Fig. 2, available at www.jneurosci.org as supplemental material). These data collectively demonstrated that K-II worked well *in vivo*, although it did not completely abolish KS.

The *in vivo* degradation of CS by C-ABC, but not that by K-II, was also confirmed by HPLC analysis (Fig. 1*B*) and Western blot analysis (Fig. 1*C*).

Motor function recovery by K-II

We next evaluated motor function recovery using the BBB score and %grip test. K-II led to a striking recovery of motor function; the effect was similar to that of C-ABC (Fig. 2*A*,*B*; supplemental Tables 1, 2, available at www.jneurosci.org as supplemental material). There was no significant difference in motor function between the K-II- and C-ABC-treated groups (Fig. 2*A*,*B*). The observed motor function recovery was confirmed by an electrophysiological technique, motor-evoked potential (MEP) monitoring, in which an electric stimulus is given at the thoracic level (Th7), and a response is taken at the gastrocnemius muscles (Fig. 2*C*; supplemental Table 3, available at www.jneurosci.org as supplemental material). K-II also showed significant functional recovery after SCI even at lower doses, e.g., as low as 2000× dilution (Fig. 2*D*; supplemental Table 4, available at www.jneurosci.org as supplemental material). No significant differences were observed between the K-II-, K-II (10× dilution)-, and K-II (2000× dilution)-treated groups (Fig. 2*D*). Consistent with this finding, K-II and K-II (2000× dilution) decreased disulfated KS contents in the spinal cord to similar extents (Fig. 1*A*). This functional recovery was due to the enzymatic activity of K-II, as heat-inactivated K-II did not promote motor function recovery at all (Fig. 2*E*; supplemental Table 4, available at www.jneurosci.org as supplemental material).

Interestingly, even though K-II or C-ABC treatment promoted the recovery of motor function, the combination of these two enzymes showed neither additive nor synergistic effects (Fig. 2*C*,*F*; supplemental Tables 3, 5, available at www.jneurosci.org as supplemental material).

Sensory function recovery by K-II

SCI induced thermal hyperalgesia and mechanical allodynia (Fig. 3*A*,*B*). The tail-immersion test and touch test showed that thermal hyperalgesia and mechanical allodynia were ameliorated by K-II or C-ABC treatment, reaching an almost normal level 10 weeks after injury (Fig. 3*A*,*B*). sp-SCEP, in which an epidural electric stimulus was given at the Th11 level and a response was taken at the Th7 level, was performed 8 weeks after injury. The results of this test support the idea that the sensory function was recovered by K-II or C-ABC treatment (Fig. 3*C*). The reinjury of K-II-treated rats lost the recovered response of sp-SCEP (Fig. 3*C*), and the results were consistent with those of previous reports (Rapalino et al., 1998; Bradbury et al., 2002).

As seen in motor function recovery, the combination of K-II and C-ABC showed neither additive nor synergistic effects on sensory function recovery (Fig. 3*C*,*D*).

Histological analysis of functional recovery after SCI

We reconstructed the serial section of the spinal cord using all of the 50–60 serial longitudinal sections per rat and estimated the number of fibers strained for GAP-43 or 5-HT. The GAP-43 and 5-HT data from the vehicle and treated groups were compared with sham-lesioned controls and expressed as a percentage along the longitudinal axis of the spinal cord (Fig. 4*A*,*B*). We found that GAP-43 staining was significantly enhanced in both the rostral and caudal regions in K-II or C-ABC-treated rats compared with vehicle control rats (Fig. 4*B*). The raphespinal tract is partly responsible for motor function in rodents, and consists of serotonin (5-HT)-positive fibers. 5-HT staining showed a striking decrease in 5-HT-positive fibers in the rostral region, especially in vehicle control rats, but K-II and C-ABC significantly increased the number of stained fibers (Fig. 4*B*). On the other hand, in the caudal region, vehicle controls showed almost no stained fibers, whereas K-II and C-ABC significantly increased the number of stained fibers (Fig. 4*B*). Representative photos of GAP-45 and 5-HT staining around the lesion were presented in Figure 4*C*. These results are consistent with the idea that K-II or C-ABC significantly promoted axonal regrowth after SCI.

Furthermore, we performed anterograde labeling of CST to evaluate axonal growth and sprouting. In tracer fiber counts for the CST, we found many fibers stained in the region rostral to the epicenter (supplemental Fig. 3, available at www.jneurosci.org as supplemental material). There was no difference among the three groups in the rostral region (Fig. 4*D*). BDA-positive fibers were barely detectable in the caudal region of the vehicle group (Fig. 4*D*,*E*). These findings support the idea that this contusion model almost completely destroyed CST at the epicenter, and thus BDA-

←

(*Figure legend continued.*) axons 10 mm rostral to the lesioned site. No significant difference was observed between treatment groups. The bottom graph represents the ratio of labeled corticospinal axons 4 and 10 mm caudal versus 10 mm rostral to the lesioned site. K-II-treated rats had significantly more BDA-positive fibers at 4 and 10 mm caudal to the lesioned site than vehicle-treated rats. Data represent the means ± SEM. $*p < 0.05$; $**p < 0.005$ versus the vehicle control ($n = 7$ Vehicle; $n = 6$ C-ABC; $n = 5$ K-II). ***E***, Representative axial sections of the spinal cord taken from 10 mm caudal from the lesioned site at 10 weeks after SCI. The boxed areas are magnified on the right side of the panel. BDA-positive fibers were clearly seen in the section of K-II-treated rat (arrows). Scale bars, 500 μm for the left panel; 100 μm for the right panels. The thin silicone tube of an osmotic mini-pump (*) remained at a point 10 mm caudal from the epicenter. WM, White matter; GM, gray matter.

positive fibers hardly passed through the lesion to the caudal region in the vehicle group. In contrast, in K-II- and C-ABC-treated rats, the number of BDA-positive fibers was significantly increased in the region caudal to the epicenter, particularly in the gray matter in this region (Fig. 4*D*,*E*). These BDA-positive fibers in the gray matter may reflect growth or sprouting of proximal or spared axons.

Restoration of neurite outgrowth by K-II

Proteoglycans purified from the brains of chicks contain both KS and CS. We previously determined 300 ng/ml as the appropriate concentration of proteoglycans to coat dishes, which did not affect cell attachment but inhibited neurite outgrowth (Ito et al., 2010). Accordingly, the substratum coated with these proteoglycans strongly inhibited neurite outgrowth (Fig. 5*A*,*B*), whereas cell binding to the substratum was comparable between conditions tested (Fig. 5*A*). The proteoglycan-mediated inhibition of neurite growth was blocked by K-II and C-ABC, and the effects of K-II and C-ABC were comparable to each other, and also consistent with our previous study (Ito et al., 2010). To our surprise, the combination of K-II and C-ABC showed neither synergistic nor additive effects (Fig. 5*B*). Thus, these *in vitro* results were consistent with the *in vivo* phenomena. We also found that heat-denatured proteoglycans as well as reduced/alkylated proteoglycans lost their inhibitory activity (Fig. 5*C*), suggesting that the conformation of the core protein structure is also essential to this inhibition, since proteins rather than sugar chains are labile to heat or reduction/alkylation.

As K-II digests KS into oligosaccharides that are each composed of two to four saccharides, we addressed whether or not these degradation products of KS reversed the proteoglycan-mediated inhibition of neurite growth. However, KS-derived oligosaccharides (Fig. 5*D*) showed no promotion of neurite growth (Fig. 5*E*). These results exclude the possibility that the K-II-induced degradation products of KS promote neurite outgrowth, and suggest that K-II directly blocks the inhibition of neurite outgrowth by proteoglycans.

Neurite growth inhibition by KS/CSPG

Based on these *in vivo* and *in vitro* results, we hypothesized that K-II and C-ABC work on the same axis. We chose aggrecan as a model molecule, as it harbors both KS and CS chains (Fig. 6*A*) and is a representative proteoglycan in the CNS. Aggrecan strikingly inhibited axonal outgrowth

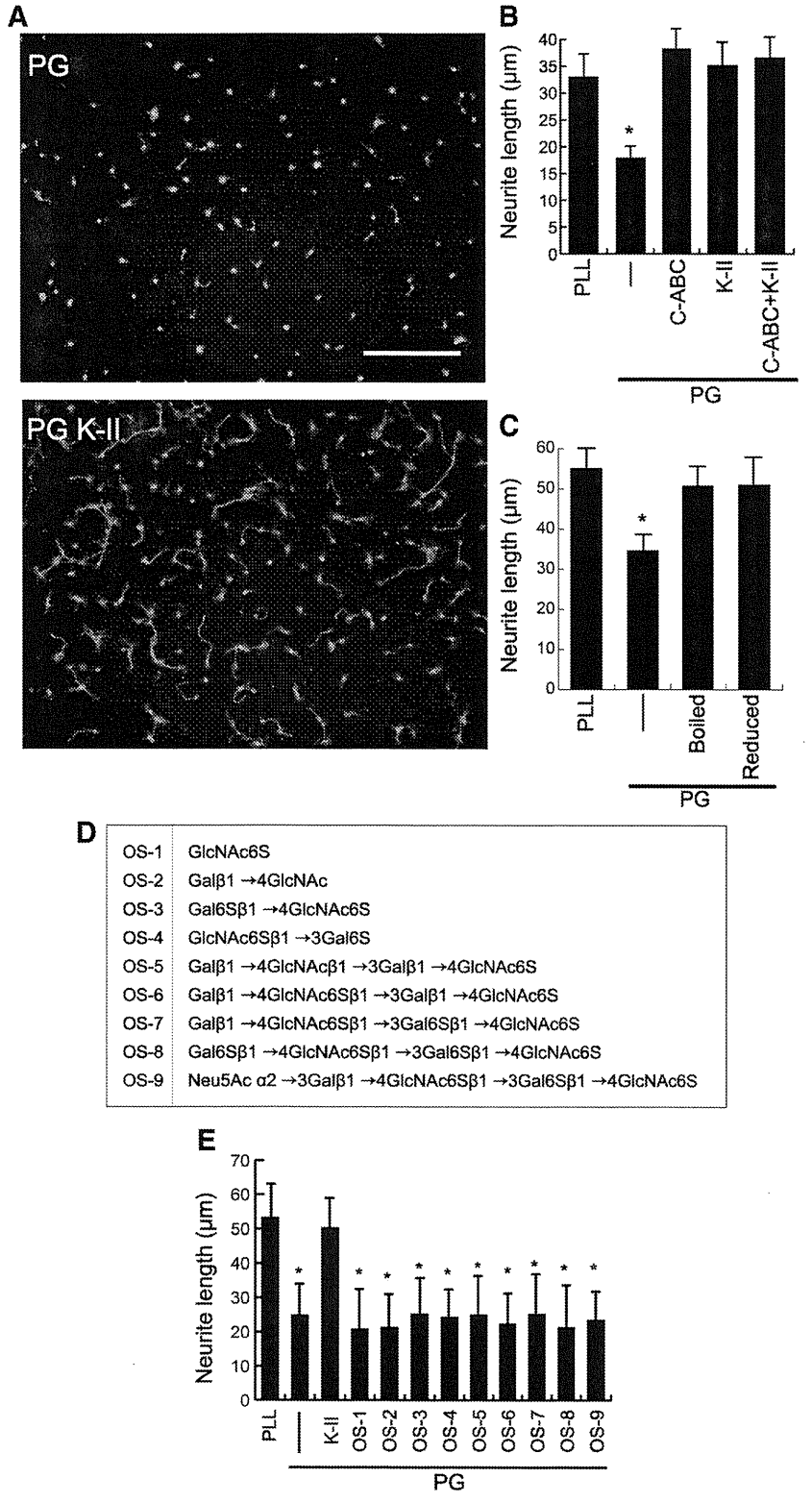

Figure 5. Restoration of neurite outgrowth by K-II. ***A***, P8 rat cerebellar granular neurons were cultured on proteoglycan (PG) extracted from chick brains. K-II treatment restored neurite outgrowth (PG K-II). Scale bar, 100 μm. ***B***, The quantification of ***A***. *$p < 0.05$ versus PLL. PG (300 ng/ml), C-ABC (200 mU/ml), and K-II (5 mU/ml) were used. Data represent the average neurite length ± SD. ***C***, Heat-denatured PG lost its neurite outgrowth-inhibitory activity. Data represent the average neurite length ± SD. *$p < 0.05$ versus PLL. ***D***, Structures of the oligosaccharides used in this experiment. ***E***, P8 rat cerebellar granular neurons were cultured on chick brain PG substrate in the absence or presence of oligosaccharides (1 μg/ml). Data represent the average neurite lengths ± SD. *$p < 0.05$ versus PLL.

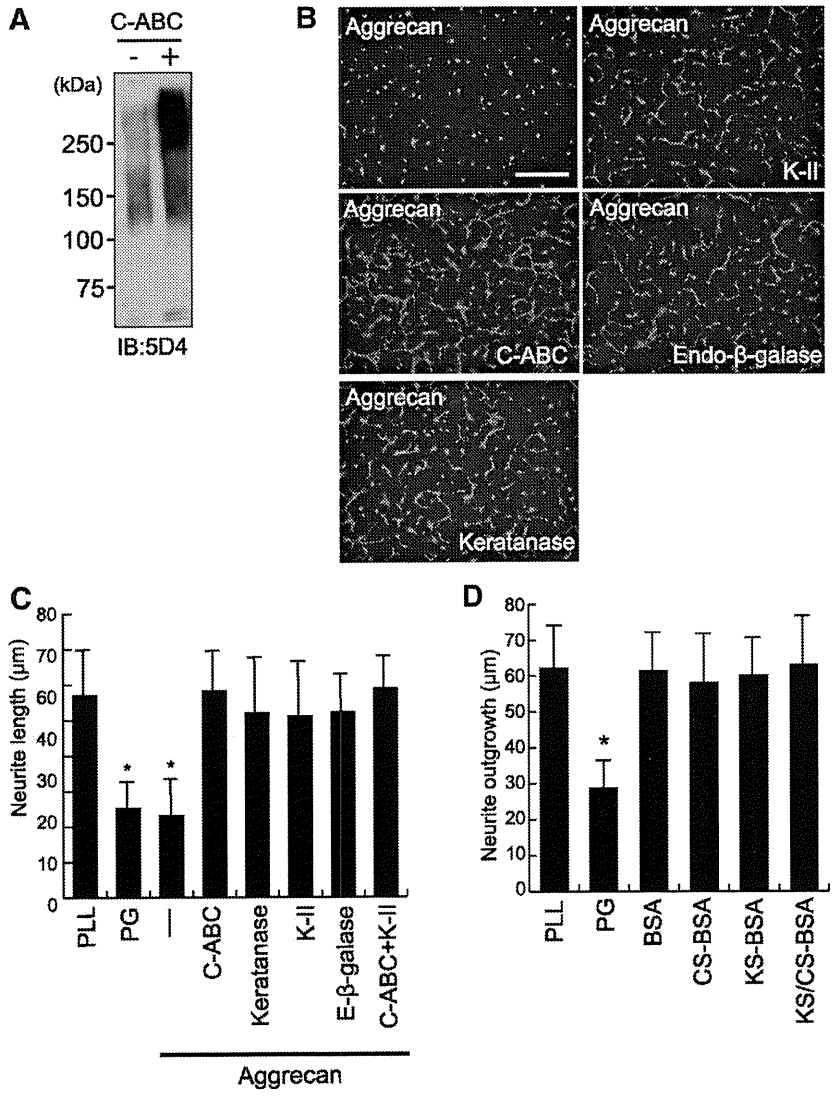

Figure 6. Effects of KS/CSPGs on neurite outgrowth. ***A***, Bovine aggrecan was digested with C-ABC (500 mU/ml) and subjected to SDS-PAGE using 5D4. Note that C-ABC treatment exposed KS epitopes. ***B***, P8 rat cerebellar granule neurons were cultured on aggrecan (5 μg/ml). Degradation of CS or KS restored neurite outgrowth. Scale bar, 100 μm. ***C***, The quantification of ***B***. Data represent the average neurite length ± SD. *$p < 0.05$ versus PLL. ***D***, There was no inhibition of neurite outgrowth by CS-BSA, KS-BSA, or KS/CS-BSA (300 ng/ml each). Data represent the average neurite length ± SD. *$p < 0.05$ versus PLL.

(Fig. 6*B*,*C*), consistent with previous studies (Asher et al., 1995; Johnson et al., 2002). The inhibition by aggrecan was as strong as that by a mixture of proteoglycans (Fig. 6*C*). Interestingly, this inhibition was reversed by C-ABC as well as K-II. Furthermore, the combination of these enzymes did not show additive or synergistic effects (Fig. 6*C*).

While K-II digested monosulfated and disulfated KS, keratanase digested monosulfated KS but not disulfated KS. The latter also reversed aggrecan-mediated inhibition of neurite outgrowth (Fig. 6*B*,*C*). Endo-β-galactosidase, which digests KS and polylactosamine, provided the same effect (Fig. 6*B*,*C*). These results collectively indicate that KS of aggrecan is required for the aggrecan-mediated inhibition of neurite outgrowth.

We then generated an artificial proteoglycan consisting of BSA, KS, and CS. In this experiment, we tried to understand how the three components of KS/CSPG (core protein, CS chains, and KS chains) are needed to exert the inhibitory activity. The estimated ratios of the core protein (BSA), CS, and KS in KS/CS-BSA were 1:30:84. Because the ratio in human aggrecan is 1:100:60 (Kiani et al., 2002), KS/CS-BSA was considered suitable for examining the function of KS, CS, and the core protein. However, KS/CS-BSA failed to inhibit neurite outgrowth (Fig. 6*D*). KS-BSA and CS-BSA also failed to do so (Fig. 6*D*).

Discussion

So far, KSPGs and CSPGs have been studied independently, and KSPGs have not been extensively studied. Our study has integrated KS and CS into a common axis. K-II and C-ABC strikingly promoted functional recovery after SCI. GAP-43, 5-HT staining, and CST tracer fiber count were significantly enhanced in K-II- or C-ABC-treated rats compared with vehicle control rats. Although the striking functional recovery may not be necessarily consistent with the data from the histological analyses, this may have been partly due to the limited ability to detect outgrowing axons by the antibodies and the tracer compound used. We found that the effects of K-II and C-ABC on *in vivo* functional disturbance after SCI and *in vitro* neurite outgrowth inhibition mediated by proteoglycans were comparable to each other. However, both *in vivo* and *in vitro*, the combination of these two enzymes showed neither additive nor synergistic effects. It should be noted that the peptide linkage region for CS always consists of xylose, galactose, and glucuronic acid, whereas the KS chain is elongated from ordinary *N*-linked or *O*-linked sugar chains. Thus, each glycosaminoglycan exists as an independent sugar chain. For example, human aggrecan is composed of a core protein and CS and KS chains at a ratio of 1:100:60 (Kiani et al., 2002). Together, our study has established that KS and CS are independently required for the inhibition of postinjury neural plasticity and neurite outgrowth.

Furthermore, we found that neurite outgrowth was not inhibited by heat-denatured proteoglycans or by reduced/alkylated proteoglycans. This inhibition was also not achieved by an artificial KS/CSPG, KS/CS-albumin, whereas the natural KS/CSPG aggrecan inhibited neurite outgrowth. Our results thus far obtained are summarized in Figure 7*A*. Our data suggest that the three components (KS, CS, and core protein) of the proteoglycan moiety are interdependent and required for proteoglycan-mediated inhibition of structural rearrangement after neuronal injuries.

It is important to point out that there is a much smaller amount of KS than CS in the CNS, and our data supported this idea (Fig. 1*B*,*C*). The family of KSPGs is also smaller than that of CSPGs (Margolis and Margolis, 1993; Funderburgh, 2000, 2002). In this context, it was surprising to us that K-II shows activity

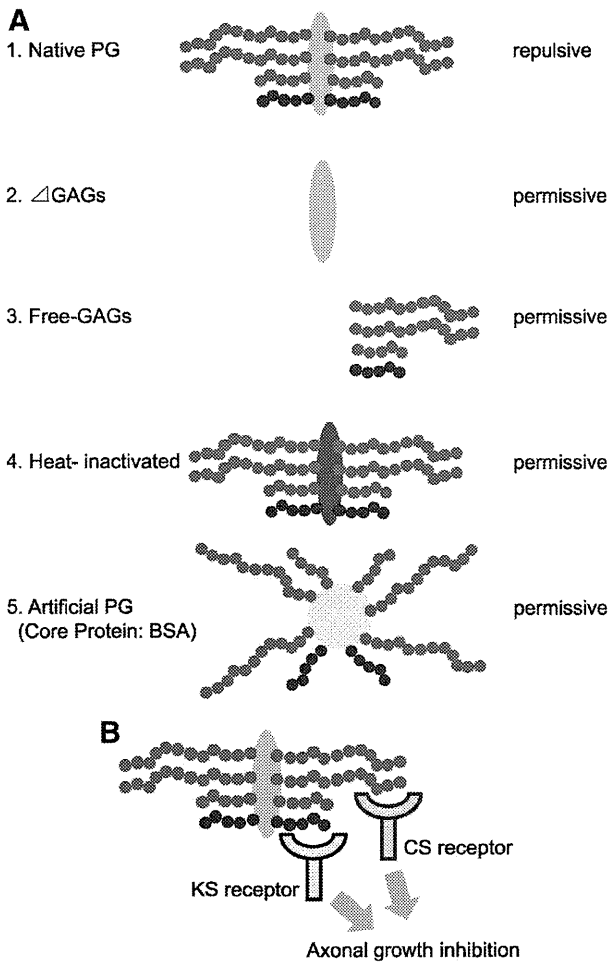

Figure 7. Structure and function relationship in the proteoglycan (PG)-mediated inhibition of neurite growth. ***A***, The present study has revealed that KS and CS have a comparable impact on PG-mediated inhibition of neurite growth. Considering our previous results that neither KS nor CS is sufficient for neurite growth inhibition (Ito et al., 2010), our data suggest that all three components of the proteoglycans moiety (core protein, CS, and KS) are required for this inhibition activity. ***B***, This scheme shows a speculated mechanism underlying the PG-mediated inhibition of axonal growth.

comparable to that of C-ABC *in vivo* and *in vitro*. Although further investigations are needed, we speculate the following mechanism (summarized in Fig. 7*B*), based on our observations. First, although KS is composed of repeating disaccharide units, the composition is heterogeneous, i.e., there are highly sulfated disaccharide clusters as well as poorly sulfated disaccharide clusters in a KS chain. Therefore, it is conceivable that there is a functional domain in a KS chain (e.g., a highly sulfated stretch of 6–8 saccharides). This is also the case in a CS chain (there are 4 different sulfation variations in CS—CS-A, -C, -D, and -E units). Second, these functional domains may appear more frequently in KS than in CS. Finally, these functional domains may be recognized independently by specific receptors so that KS and CS are independently required for the inhibition of neurite outgrowth (Fig. 7*B*). Our idea is partly supported by the recent report that PTPσ is the receptor for CS (Shen et al., 2009; Coles et al., 2011). However, there is another possibility. C-ABC might not be very stable, although a significant portion of CS appeared to be lost by C-ABC treatment on Western blot analysis (Fig. 1*C*). Thus, we should not exclude the possibility that an insufficient *in vivo* digestion of CS by our current method led to the lack of synergism of K-II and C-ABC.

Reported data regarding the biological impacts of KS and CS on neurite outgrowth have been contradictory. For example, Powell et al. (1997) reported *in vitro* data that showed the effects of CS and KS are similar, but that enzymatic treatment with C-ABC and keratanase is synergistic. In contrast, Snow et al. (1990b) showed that *in vitro* enzymatic removal of KS and CS from CSPGs differ with regard to neurite behavior (CS is stronger than KS). Furthermore, in cultured hippocampal slices, keratanase, but not C-ABC, leads to misrouting of mossy fibers (Butler et al., 2004). In the present study, we conducted experiments both *in vivo* and *in vitro* to address the same issue. Our study has revealed that KS and CS are independent requirements for the proteoglycan-mediated inhibition of postinjury neural plasticity *in vivo*. Taking into account that the K-II used for *in vivo* experiments in the present study is relatively stable at 37°C and has a wide window of therapeutic doses, our *in vivo* data may be reliable. *In vitro* results were consistent with *in vivo* data. Although discrepancy between reports might be due to different conditions examined, our results may provide a hint for further studies on molecular mechanisms of the neural plasticity regulation by proteoglycans.

The functional recovery by K-II or C-ABC after SCI may not simply rely on neurite outgrowth promotion by these enzymes. The ECM surrounding neurons forms a lace-like structure, the so-called perineuronal net (Takahashi-Iwanaga et al., 1998), and is essentially composed of hyaluronic acid and proteoglycans. Perineuronal nets are prominent on GABAergic interneurons, but can be detected on virtually all neurons (Celio and Blümcke, 1994; Celio et al., 1998; John et al., 2006). This ECM may inhibit structural rearrangements at synapses, thereby contributing to the maintenance of neuronal networks; this idea is supported by recent works showing that C-ABC promotes synaptic plasticity and dendritic spine dynamics (Pizzorusso et al., 2002, 2006; Berardi et al., 2004; Oray et al., 2004). C-ABC restores the plasticity of not only sensory networks but also emotional networks (Pizzorusso et al., 2002; Gogolla et al., 2009). Furthermore, hyaluronidase, a hyaluronic acid-degrading enzyme, and C-ABC increase AMPA receptor lateral mobility, and consequently modulate short-term synaptic plasticity (Frischknecht et al., 2009). Considering these data together, our results suggest that K-II and C-ABC may remove the ECM and promote structural rearrangement of neuronal networks after SCI. In this context, it is an interesting challenge to ask whether K-II also restores ocular dominance plasticity in adults.

Regarding the lateral mobility of membrane molecules such as AMPA receptor on dendrites, the ECM works as a viscous diffusion constraint that slows and confines the mobility of molecules entering the ECM-covered compartments (Frischknecht et al., 2009). Thus, a general function of the ECM is to act as a passive barrier. On the other hand, it has recently been reported that PTPσ acts as a receptor for CS and mediates the inhibitory activity of CSPGs on axonal regeneration (Shen et al., 2009). Our data raise the intriguing possibility that a KS-specific receptor may also exist (Fig. 7*B*).

It is also important to consider that KS degradation within the intact area may cause maladaptive plasticity if K-II affects the ECM structure. However, as shown in Figure 3, K-II administration promoted recovery from thermal hyperalgesia and mechanical allodynia. Thus, the delivery method used in our study could minimize the unwanted adverse effect of KS degradation. Supporting this idea, we observed that *in vivo* KS degradation by K-II

was good enough to promote functional recovery, but not completely abolish KS, probably due to a limited diffusion of infused enzyme.

In addition to the therapeutic effects of K-II on SCI, we also noticed that the functional recovery induced by K-II or C-ABC was not complete. Therefore, further improvement of a therapeutic strategy for SCI must be considered. García-Alías et al. (2009) recently reported that a combination of C-ABC and rehabilitation leads to a striking functional recovery after SCI at the cervical level. Even if our present results suggest that K-II or C-ABC may promote not only axonal regrowth but also neural plasticity related to motor and sensory function, other efforts, such as rehabilitation, to improve the reestablishment of neural circuitry would be helpful to realize a satisfactory treatment for SCI.

References

Asher RA, Scheibe RJ, Keiser HD, Bignami A (1995) On the existence of a cartilage-like proteoglycan and link proteins in the central nervous system. Glia 13:294–308.

Basso DM, Beattie MS, Bresnahan JC (1995) A sensitive and reliable locomotor rating scale for open field testing in rats. J Neurotrauma 12:1–21.

Berardi N, Pizzorusso T, Maffei L (2004) Extracellular matrix and visual cortical plasticity: freeing the synapse. Neuron 44:905–908.

Bradbury EJ, Moon LD, Popat RJ, King VR, Bennett GS, Patel PN, Fawcett JW, McMahon SB (2002) Chondroitinase ABC promotes functional recovery after spinal cord injury. Nature 416:636–640.

Butler CD, Schnetz SA, Yu EY, Davis JB, Temple K, Silver J, Malouf AT (2004) Keratan sulfate proteoglycan phosphacan regulates mossy fiber outgrowth and regeneration. J Neurosci 24:462–473.

Celio MR, Blümcke I (1994) Perineuronal nets—a specialized form of extracellular matrix in the adult nervous system. Brain Res Brain Res Rev 19:128–145.

Celio MR, Spreafico R, De Biasi S, Vitellaro-Zuccarello L (1998) Perineuronal nets: past and present. Trends Neurosci 21:510–515.

Cole GJ, McCabe CF (1991) Identification of a developmentally regulated keratan sulfate proteoglycan that inhibits cell adhesion and neurite outgrowth. Neuron 7:1007–1018.

Coles CH, Shen Y, Tenney AP, Siebold C, Sutton GC, Lu W, Gallagher JT, Jones EY, Flanagan JG, Aricescu AR (2011) Proteoglycan-specific molecular switch for RPTPσ clustering and neuronal extension. Science 332:484–488.

Davies SJ, Goucher DR, Doller C, Silver J (1999) Robust regeneration of adult sensory axons in degenerating white matter of the adult rat spinal cord. J Neurosci 19:5810–5822.

Frischknecht R, Heine M, Perrais D, Seidenbecher CI, Choquet D, Gundelfinger ED (2009) Brain extracellular matrix affects AMPA receptor lateral mobility and short-term synaptic plasticity. Nat Neurosci 12:897–904.

Funderburgh JL (2000) Keratan sulfate: structure, biosynthesis, and function. Glycobiology 10:951–958.

Funderburgh JL (2002) Keratan sulfate biosynthesis. IUBMB Life 54:187–194.

García-Alías G, Barkhuysen S, Buckle M, Fawcett JW (2009) Chondroitinase ABC treatment opens a window of opportunity for task-specific rehabilitation. Nat Neurosci 12:1145–1151.

Geisert EE Jr, Bidanset DJ, Del Mar N, Robson JA (1996) Up-regulation of a keratan sulfate proteoglycan following cortical injury in neonatal rats. Int J Dev Neurosci 14:257–267.

Gogolla N, Caroni P, Lüthi A, Herry C (2009) Perineuronal nets protect fear memories from erasure. Science 325:1258–1261.

Grimpe B, Silver J (2004) A novel DNA enzyme reduces glycosaminoglycan chains in the glial scar and allows microtransplanted dorsal root ganglia axons to regenerate beyond lesions in the spinal cord. J Neurosci 24:1393–1397.

Hutchinson KJ, Gómez-Pinilla F, Crowe MJ, Ying Z, Basso DM (2004) Three exercise paradigms differentially improve sensory recovery after spinal cord contusion in rats. Brain 127:1403–1414.

Ito Z, Sakamoto K, Imagama S, Matsuyama Y, Zhang H, Hirano K, Ando K, Yamashita T, Ishiguro N, Kadomatsu K (2010) *N*-acetylglucosamine 6-*O*-sulfotransferase-1-deficient mice show better functional recovery after spinal cord injury. J Neurosci 30:5937–5947.

John N, Krügel H, Frischknecht R, Smalla KH, Schultz C, Kreutz MR, Gundelfinger ED, Seidenbecher CI (2006) Brevican-containing perineuronal nets of extracellular matrix in dissociated hippocampal primary cultures. Mol Cell Neurosci 31:774–784.

Johnson WE, Caterson B, Eisenstein SM, Hynds DL, Snow DM, Roberts S (2002) Human intervertebral disc aggrecan inhibits nerve growth in vitro. Arthritis Rheum 46:2658–2664.

Jones LL, Tuszynski MH (2002) Spinal cord injury elicits expression of keratan sulfate proteoglycans by macrophages, reactive microglia, and oligodendrocyte progenitors. J Neurosci 22:4611–4624.

Kiani C, Chen L, Wu YJ, Yee AJ, Yang BB (2002) Structure and function of aggrecan. Cell Res 12:19–32.

Krautstrunk M, Scholtes F, Martin D, Schoenen J, Schmitt AB, Plate D, Nacimiento W, Noth J, Brook GA (2002) Increased expression of the putative axon growth-repulsive extracellular matrix molecule, keratan sulphate proteoglycan, following traumatic injury of the adult rat spinal cord. Acta Neuropathol 104:592–600.

Margolis RK, Margolis RU (1993) Nervous tissue proteoglycans. Experientia 49:429–446.

Massey JM, Hubscher CH, Wagoner MR, Decker JA, Amps J, Silver J, Onifer SM (2006) Chondroitinase ABC digestion of the perineuronal net promotes functional collateral sprouting in the cuneate nucleus after cervical spinal cord injury. J Neurosci 26:4406–4414.

Moon LD, Asher RA, Rhodes KE, Fawcett JW (2001) Regeneration of CNS axons back to their target following treatment of adult rat brain with chondroitinase ABC. Nat Neurosci 4:465–466.

Moon LD, Asher RA, Rhodes KE, Fawcett JW (2002) Relationship between sprouting axons, proteoglycans and glial cells following unilateral nigrostriatal axotomy in the adult rat. Neuroscience 109:101–117.

Oray S, Majewska A, Sur M (2004) Dendritic spine dynamics are regulated by monocular deprivation and extracellular matrix degradation. Neuron 44:1021–1030.

Pizzorusso T, Medini P, Berardi N, Chierzi S, Fawcett JW, Maffei L (2002) Reactivation of ocular dominance plasticity in the adult visual cortex. Science 298:1248–1251.

Pizzorusso T, Medini P, Landi S, Baldini S, Berardi N, Maffei L (2006) Structural and functional recovery from early monocular deprivation in adult rats. Proc Natl Acad Sci U S A 103:8517–8522.

Powell EM, Fawcett JW, Geller HM (1997) Proteoglycans provide neurite guidance at an astrocyte boundary. Mol Cell Neurosci 10:27–42.

Properzi F, Carulli D, Asher RA, Muir E, Camargo LM, van Kuppevelt TH, ten Dam GB, Furukawa Y, Mikami T, Sugahara K, Toida T, Geller HM, Fawcett JW (2005) Chondroitin 6-sulphate synthesis is up-regulated in injured CNS, induced by injury-related cytokines and enhanced in axon-growth inhibitory glia. Eur J Neurosci 21:378–390.

Pumphrey CY, Theus AM, Li S, Parrish RS, Sanderson RD (2002) Neoglycans, carbodiimide-modified glycosaminoglycans: a new class of anticancer agents that inhibit cancer cell proliferation and induce apoptosis. Cancer Res 62:3722–3728.

Rapalino O, Lazarov-Spiegler O, Agranov E, Velan GJ, Yoles E, Fraidakis M, Solomon A, Gepstein R, Katz A, Belkin M, Hadani M, Schwartz M (1998) Implantation of stimulated homologous macrophages results in partial recovery of paraplegic rats. Nat Med 4:814–821.

Shen Y, Tenney AP, Busch SA, Horn KP, Cuascut FX, Liu K, He Z, Silver J, Flanagan JG (2009) PTPσ is a receptor for chondroitin sulfate proteoglycan, an inhibitor of neural regeneration. Science 326:592–596.

Shinmei M, Miyauchi S, Machida A, Miyazaki K (1992) Quantitation of chondroitin 4-sulfate and chondroitin 6-sulfate in pathologic joint fluid. Arthritis Rheum 35:1304–1308.

Silver J, Miller JH (2004) Regeneration beyond the glial scar. Nat Rev Neurosci 5:146–156.

Sivasankaran R, Pei J, Wang KC, Zhang YP, Shields CB, Xu XM, He Z (2004) PKC mediates inhibitory effects of myelin and chondroitin sulfate proteoglycans on axonal regeneration. Nat Neurosci 7:261–268.

Snow DM, Steindler DA, Silver J (1990a) Molecular and cellular characterization of the glial roof plate of the spinal cord and optic tectum: a possible role for a proteoglycan in the development of an axon barrier. Dev Biol 138:359–376.

Snow DM, Lemmon V, Carrino DA, Caplan AI, Silver J (1990b) Sulfated

proteoglycans in astroglial barriers inhibit neurite outgrowth *in vitro*. Exp Neurol 109:111–130.

Sutter M, Deletis V, Dvorak J, Eggspuehler A, Grob D, Macdonald D, Mueller A, Sala F, Tamaki T (2007) Current opinions and recommendations on multimodal intraoperative monitoring during spine surgeries. Eur Spine J 16 [Suppl 2]:S232–S237.

Takahashi-Iwanaga H, Murakami T, Abe K (1998) Three-dimensional microanatomy of perineuronal proteoglycan nets enveloping motor neurons in the rat spinal cord. J Neurocytol 27:817–827.

Tamaki T, Kubota S (2007) History of the development of intraoperative spinal cord monitoring. Eur Spine J 16 [Suppl 2]:S140–S146.

Tom VJ, Steinmetz MP, Miller JH, Doller CM, Silver J (2004) Studies on the development and behavior of the dystrophic growth cone, the hallmark of regeneration failure, in an *in vitro* model of the glial scar and after spinal cord injury. J Neurosci 24:6531–6539.

Yamagishi K, Suzuki K, Imai K, Mochizuki H, Morikawa K, Kyogashima M, Kimata K, Watanabe H (2003) Purification, characterization, and molecular cloning of a novel keratan sulfate hydrolase, endo-β-*N*-acetylglucosaminidase, from *Bacillus circulans*. J Biol Chem 278: 25766–25772.

Zhang H, Muramatsu T, Murase A, Yuasa S, Uchimura K, Kadomatsu K (2006) *N*-Acetylglucosamine 6-*O*-sulfotransferase-1 is required for brain keratan sulfate biosynthesis and glial scar formation after brain injury. Glycobiology 16:702–710.